U. Carlos III de Madrid

Universidad Carlos III de Madrid
www.uc3m.es

VERTEXWISE SULCAL WIDTH MAP COMPUTED OVER THE HUMAN CORTICAL SURFACE USING MAGNETIC RESONANCE IMAGING

Author: Isabel Martínez Tejada
Tutor: Manuel Desco Menéndez, PhD, MD
Supervised by: Yasser Alemán Gómez, PhD

2016

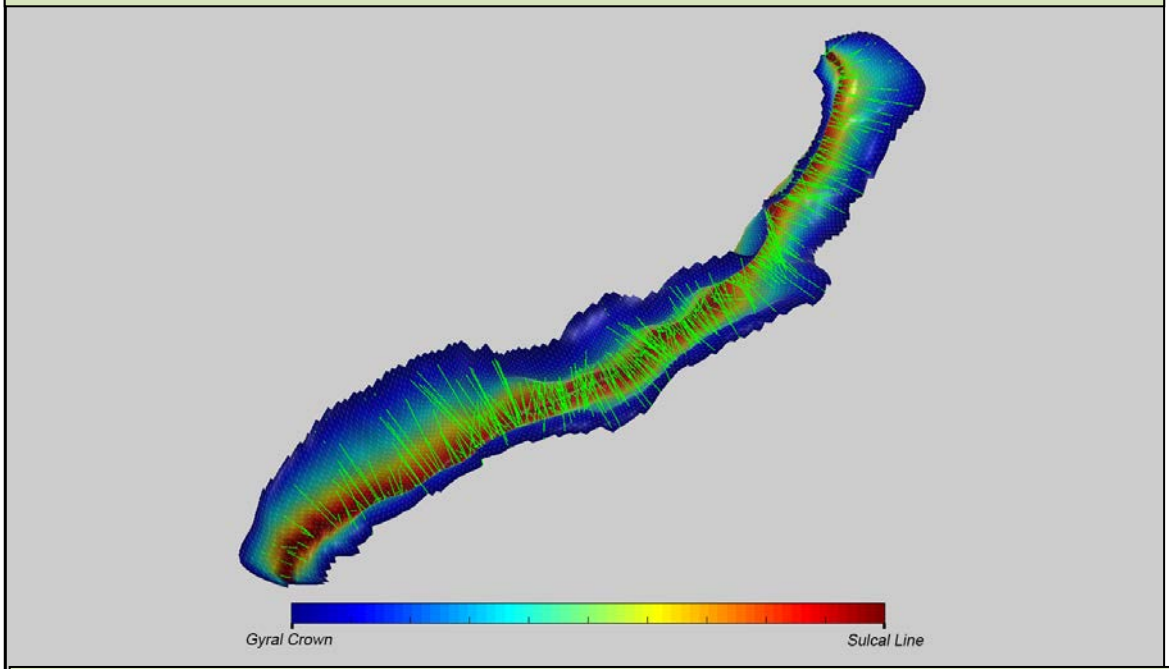

Universidad Carlos III de Madrid. Departamento de Bioingeniería e Ingeniería Aeroespacial

Agradecimientos

Quedan tan solo unas horas para entregar el Trabajo de Fin de Grado. Sin embargo, no estaría aquí sin la ayuda y el apoyo de todos aquellos que no solo han hecho que este proyecto fuera posible sino que también han hecho de él una experiencia inolvidable. En realidad, no podría ni haber empezado este proyecto de no ser por la oportunidad que Manuel Desco me brindó a principio de curso. Muchas gracias tanto a él como a Yasser Alemán por su apoyo continuo durante todos estos meses.

Aparte de a mis tutores, también quiero darle las gracias a mi familia (con mención especial a mis abuelos, ya que no hay día que no me acuerde de ellos) por quererme siempre. Y también gracias a todas aquellas personas que son como familia para mi: mis amigas Sara, Vir, Pati y Cris por compartir la vida conmigo y hacer que sea mejor; a mis amigas Elena, Tito y Cris por ser mis compañeras de vida desde que era pequeña; a mis amigas Teresa, Marina y Blanca porque si algo bueno me llevo de estos cuatros años de carrerra son ellas; y a mi novio, por su sonrisa constante y su apoyo.

Finalmente, aunque mencionado anteriormente, mi mención especial a Yasser por su paciencia, entusiasmo y enorme conocimiento, además de su continuo apoyo y orientación en todo momento. No podría haber encontrado una persona mejor con la que trabajar. Y gracias también por hacerme ver cual es el camino que quiero seguir (la neuroimagen), por no perder nunca la esperanza en que algún día la investigación sera valorada como se merece, y lo más importante, por enseñarme que al final lo más importante es ser buena persona.

Summary

The human cortex is folded into a pattern of well-defined outward folds called gyri and buried inward folds known as sulci. The shape and size of the human cortex can be quantified and these quantifications can be used as biomarkers. Biomarkers may play an important role in the diagnosis and prognosis of neurological diseases. Two shape descriptors that have been largely ignored are the distance between the sulcal banks, i.e. the sulcal width, and the top-to-bottom distance of sulci, i.e. sulcal depth. In this work, a new method is proposed for quantitative assessment of sulcal width and depth from MRI T1-weighted images. The main steps during the image processing method include: (1) the extraction of sulcal lines and gyral crowns from the anatomy of the sulcus and (2) the normalization of the cortical surface such that pattern irregularities are taken into account, and (3) the generation of a vertex-wise sulcal width and depth maps. A validation of the proposed method is presented and, in addition, an example of a potential application of the method. We foresee that the developed method is applicable to research aimed at quantifying cortical shape for clinical as well as non-clinical purposes.

Contents

List of figures

List of tables

Chapter 1: General introduction

1.1. Motivation

The cerebral cortex is folded, it is thought that this typical shape provides the brain with the possibility to pack more gray matter within the limited space of the skull. The grooves that make the wrinkles are called *sulci* (inward folds buried into the cortex) and the ridges between them are called *gyri* (outward folds). The human cerebral cortex has a high degree of folding, i.e. 2/3 of the cortical surface is buried into sulci. Study and analysis of sulcal morphology may facilitate multisubject atlasing, neurosurgical studies, and multimodality brain mapping applications.

Besides functional and cognitive information, structural neuroimaging has become a key technique for the evaluation and quantification, *in vivo*, of brain maturational changes, aging, learning or disease (Van Soelen et al., 2012). Within the domain of medical imaging, magnetic resonance imaging (MRI) is a technique that enables investigating complex spatial and functional relationships between different brain areas. Magnetic resonance is a widely available, harmless, and very flexible technique since contrast can be made sensitive to various structures.

Along with the improvements in image acquisition techniques, new methods are developed for measurement of the size and shape of biological structures. These methods are known as *brain morphometric techniques*. They provide measurements that can be used as biomarkers such as brain volume, the thickness of the cortex or the degree of cortical folding and more fine-grained ones such as sulcus width, depth or length. All of them can then be mapped on the brain cortex surface allowing for the characterization of their pattern over time and across groups.

In addition, brain morphological metrics have an important potential for the diagnosis and prognosis of neurological diseases. This is the most important reason for justifying the study of an individual's sulcal width and depth. In fact, cortical thickness estimation methods for studying brain structural changes are being either replaced or complemented more fine-grained methods focusing on sulcal metrics (Bastos-Leite et al., 2006).

Sulcal width has previously been investigated as a biomarker for Alzheimer disease. In this disease, the hippocampal sulcus was found to have significantly larger width patients compared to healthy controls, thought to be indicative of medial temporal lobe atrophy (Bastos-Leite et al., 2006). Bipolar disorder has also been linked to sulcal width abnormalities. Sulcal width in bipolar patients appeared to be wider than sulcal width in healthy subjects. This widening was larger for the superior and intermediate frontal sulci (Coyle et al., 2006). Furthermore, sulcal width irregularities are also associated to multiple sclerosis. Widening of supratentorial ventricular width has been found in patients with this neurodegenerative disease (Martola et al., 2008).

Since cortical morphology metrics can be used as biomarkers for multiple neurodegenerative diseases, their quantitative estimation has been of special interest for researchers and neuroscientists throughout the past decade. Nevertheless, the automatic calculation of both sulcal width and sulcal depth is a field largely unexplored. In fact, none of the previous published works focus on how sulcal width changes across the cortical surface. Its calculation is based on an average over the surface of an a priori selected anatomical region. This approach leads to a loss of local information about how sulcal width changes across the brain cortical surface. These reasons explain why a new methodology, which allows for a subregional (submillimetre) estimation of sulcal width and depth, is needed.

In order to quantitatively estimate these biomarkers two main steps are required: 1) the extraction of sulcal lines and gyral crowns and 2) sulcal width and depth cortical maps computation. The first step is computed following previously developed methodology. However, the second step is the basis of this TFG. The obtained cortical maps will provide new biomarkers that could be employed for research in neurodegenerative diseases. For the first time they will be calculated on a point-by-point basis, which will allow for a point-wise morphometric analysis of the human brain cortex.

1.2. Socioeconomic background for the project

Neurodegenerative diseases represent a real problem in terms of economic cost and human suffering. They are difficult to treat conditions that debilitate the patient and often have poor prognosis. Therefore, these disorders are strongly linked with age. The problem aggravates when taking into account that world's population is aging, which

implies that a higher percentage of the population is going to suffer from one of these diseases. In 2013 there were 841 million people over 60 years. This number is estimated to increase to at least 2 billion in 2050 (Johnson, 2015), which implies that more people will suffer from a neurodegenerative disorder. For example, the number of people with Alzheimer disease is expected to rise up from 26.6 million in 2011 to 106.2 million in 2050 (Herrmann et al., 2015).

Along with the increasing percentage of the population with a neurodegenerative disease, the cost of taking care of these patients is also rising. A study estimates the global cost of dementia to be $604 billion in 2010, including healthcare, social services and informal care (Morris et al., 2015). When compared with the cost of other conditions such as cancer or heart disease, the difference is noticeable. Cancer costs $77 billion while heart diseases cost $102 billion (Hurd et al., 2013).

The key for reducing these costs lies in the prevention of neurodegenerative diseases, especially now that the trend of people suffering them is in exponential growth. The results obtained in this Project may provide tools for new imaging studies of disease prevention or early detection. The possible applications could focus on the research of cortical biomarkers changes as the onset factor of the disease. The patient evolution could also be followed based on these biomarkers.

1.3. Hypothesis and objectives

Hypothesis

Vertexwise sulcal width values will provide local information about how this morphological property changes across the human brain cortex.

Objectives

The first objective is to develop a methodology that allows for computing a vertexwise sulcal width map over the human cortical surface using MRI. This objective can be divided into three subgoals:

a. Divide each sulcal basin in different regions according to their anatomical topology using previously extracted sulcal lines and gyral crowns.
b. Compute sulcal depth maps for each region
c. Create sulcal width maps

The final objective is to compare results of the developed method with those of previous methods.

1.4. Author's contributions

The contributions by the student presenting this report are listed below:

- Bibliographical search on MRI and brain morphometry backgrounds as well as previous work on sulcal width maps' calculation (Chapter 2).
- Extraction of sulcal lines and gyral crowns in order to use them as input for the algorithm developed (Chapter 3.4).
- Development of a methodology to calculate vertexwise sulcal width maps (Chapter 3.2 to Chapter 3.7).
- Validation of the developed sulcal width maps algorithm (Chapter 4).

1.5. Budget

The estimated expenses for this Project are outlined in the following table:

Concept	Number of subjects	Cost	Total (€)
Image acquisition	85	300€/subject	25,500
Image processing and quantification	85	250€/subject	21,250
Personal	4 Person/month	1PM = 3,000€	12,000
Other goods and services			10,000
Total direct costs			68,750
Indirect costs (21%)			14,438
Total costs			83,188

Table 1.1: *Estimated project budget.*

1.6. Outline

Content information in this project is broken down into five different chapters. First of all, **Chapter 1: General introduction** explains the motivation for the work done, sets the main objectives needed to reach so as to find an answer for the stated

hypothesis, provides a brief socioeconomic background of the work and also lists the author's contributions. The following chapter, **Chapter 2: Introduction and previous work**, gives some background on MRI techniques, brain anatomy and its corresponding morphometry so as to create a context for the following chapters. In addition, the state of art on sulcal width computation is presented in this Chapter. The next chapter, **Chapter 3: Sulcal width computation**, explains in detail the novel methodology developed in this project, including the removal of unwanted sulcal line branches, depth map generation and the final calculation of sulcal width along the entire cortical surface, among other sections. The validation of the presented methodology (results discussion) as well as a presentation of applications of sulcal width maps is discussed in **Chapter 4: Results and discussion**. At last, **Chapter 5: Conclusions and future work** draws the conclusions of this work. It also introduces some limitations of the methodology, which could be improved in the future. The last pages are reserved for the **Related references**.

Chapter 2: Introduction and previous work

The human brain cortex is a wrinkled outer layer of the cerebrum. Its folded up gray matter surface covers the hemispheres, the two connected major lateral parts of the brain. Within each hemisphere different cortical regions have different functions that range from memories formation and storage to thoughts generation or interpretation of sensations from the outside world (Ackerman, 1992). Since a lot of complex activities are taking place at the same time inside the human brain, this organ is considered the most complex part of the entire nervous system. The complex interplay between gray matter, white matter, and most specifically cell bodies are responsible for these functions. The spatial arrangement of these cell bodies is referred to as cortical gyrification or convolution and is responsible for the presence of ridges and grooves in the cerebral cortex. Cortical folding is positively linked to cognitive abilities because it allows for a greater amount of cortical surface to fit inside the fixed skull. Folding is also very important for direct distribution of glucose and oxygen to the cell bodies, considering that most arteries are spread along the brain cortex.

A *sulcus* is the inward fold. The line that runs through the path of maximum curvature within the sulcus is referred to as *sulcal line* (see Figure 2.1). On the other hand, a *gyrus* is the outward fold. The line along the top of the gyrus is the *gyral crown line* (see Figure 2.1).

Major sulci and gyri divide each hemisphere into six lobes: frontal, occipital, parietal, temporal, insular and limbic (Fix, 1995).

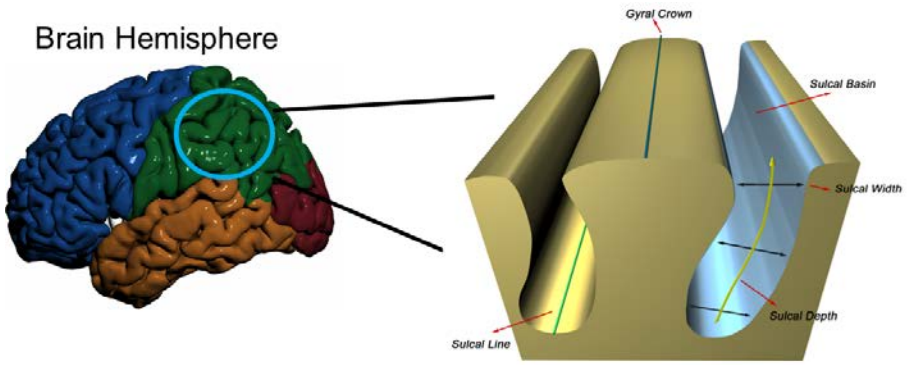

Figure 2.1: *Brain sulci and gyri scheme.*

Sulcal lines and gyral crowns need to be extracted from MRI images so as to measure how both sulcal width and sulcal depth change along the entire sulcal basin,

which are the main goals of this project, as specified in Chapter 1.3. This step is performed on *cortical surfaces* extracted from T1-weighted magnetic resonance images (T1W-MRI) because of their higher resolution and their good intensity contrast between brain tissues.

Sulcal width (see Figure 2.1B) is defined as the Euclidean distance between opposite sulcal walls; while *sulcal depth* (see Figure 2.1A) is defined as the geodesic distance between the top of the gyrus and the bottom of the sulcus, i.e. the sulcal fundus.

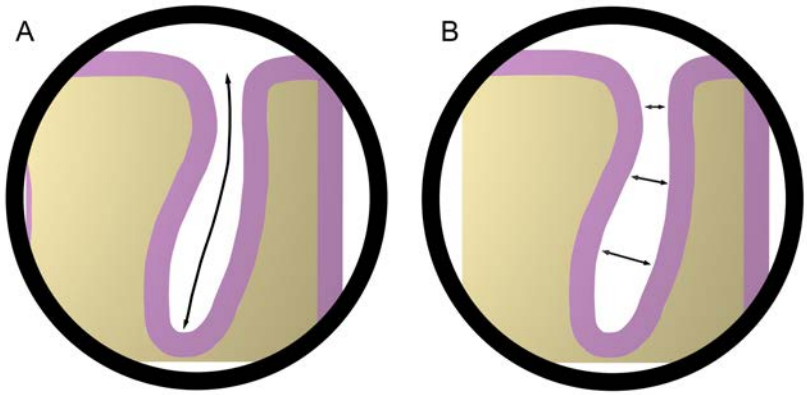

Figure 2.2: ***A)*** *Sulcal depth.* ***B)*** *Sulcal width.*

This chapter presents a brief review focusing on the most popular and commonly used methods for brain T1-weighted MRI morphometry, as well as some important image preprocessing concepts and biomarkers used to obtain an accurate structural characterization of human brain. Finally, previous works in sulcal width computation are analyzed.

2.1. Brief background on structural MRI

Magnetic resonance imaging is a medical imaging modality whose first medical applications date back to 1973. Therefore, it can be considered a recent modality (Suetens, 2009). In essence, MRI makes use of both radio waves and magnetic fields, which implies that it is a neither invasive nor ionizing (involves no radiation) technique. It's widely use in neuroimaging research is due to two factors: excellent spatial resolution and good temporal resolution, allowing in vivo characterization and quantification of brain tissue geometry: volume, surface, width, etc.

Contrast in anatomical MRI images is determined by each tissue's relaxation time. Therefore, each contrast type is different depending on the tissue. The two most important types of relaxation times are referred to as T1 and T2 (Liang et al., 2000). The effect of pondering an image in both T1 (Figure 2.3A) and T2 (Figure 2.3B) can be observed in the following image.

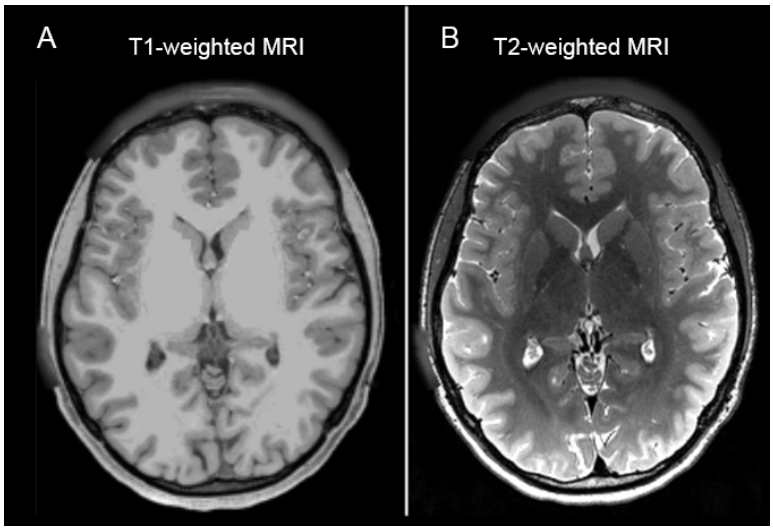

Figure 2.3: *MRI structural images.* ***A)*** *T1-weighted image.* ***B)*** *T2-weighted image.*

Differences between the two different contrasts obtained can also be observed in the previous image. On the one hand, *T1-Weighted MRI images* (T1W-MRI) have brighter intensities the more dense the tissue is (i.e. white matter), whereas the intensities are usually darker for liquid parts of the brain such as the cerebrospinal fluid (CSF). This type of image delineates gray matter, white matter and cerebrospinal fluid. On the other hand, *T2-Weighted MRI images* (TW2-MRI) are pondered exactly in the opposite way: intensities tend to be brighter for white matter, whereas for cerebrospinal fluid and gray matter they are darker. This kind of image is used for detection of tissue abnormalities.

2.2. Brief background on brain morphometry

Neuroimaging research has completely changed due to the rapid development of new methodology and technology improvement. Answers to questions such as how the brain is folded are now being found. Also, identification of markers for neurodegenerative diseases' detection is now possible since structural changes in the brain can be identified from structural MRI images.

This identification consists of automatic methods developed in the recent years. Thanks to these methods being automated, a lot of time is being saved and working with larger amounts of data is becoming viable. This implies that diagnostic procedures are shorter; so more patients can be studied. The main advantage of computerization is that radiologist experts no longer need to analyze MRI sequences for any pathological abnormalities nor perform any manual measurements to obtain data from the regions of interest (ROIs). The most important methods are two: *Voxel Based Morphometry* (VBM) and *Surface Based Morphometry* (SBM). This Project will focus on the work with surfaces (SBM).

This technique involves two main steps: tissue segmentation and mesh creation. The first one has the objective of generating white matter (WM), gray matter (GM) and cerebrospinal fluid (CSF) from T1W-MRI images so as to define structural boundaries within the brain. The voxels in this image are classified into groups (WM, GM and CSF) depending on their intensity value (see Figure 2.4).

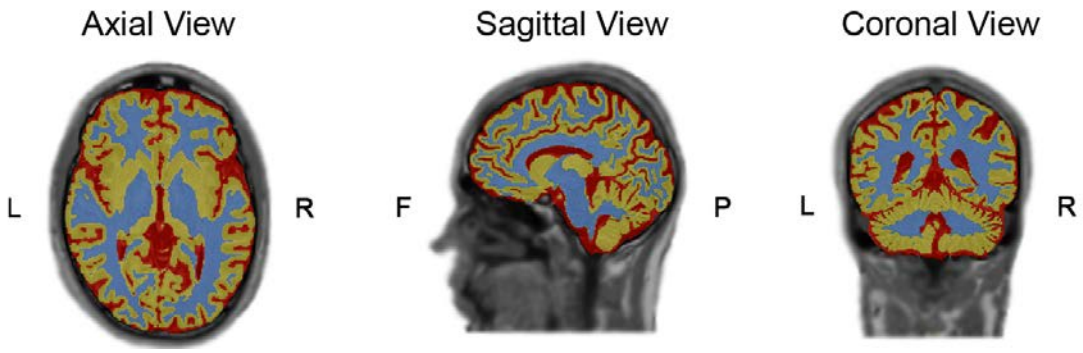

Figure 2.4: *Input T1-Weighted image and brain tissue segmentation. **Blue**: White Matter. **Red**: Cerebrospinal Fluid. **Yellow**: Gray Matter.*

The second step consists on creating a surface over gray/white and gray/CSF boundaries by a meshing algorithm. These surfaces are known as *cortical surfaces*. They are constructed by a mesh of triangles known as faces. The place where the corners of the triangles meet is called vertex (Greve, 2011). Each vertex is represented by the X, Y and Z coordinates previously obtained in the surface extraction stage. *Pial surface*, which is built from the GM and CSF boundary, and the *white surface*, extracted from the WM and GM boundary (inner boundary of the cortex), are the two examples of cortical surfaces (see Figure 2.5).

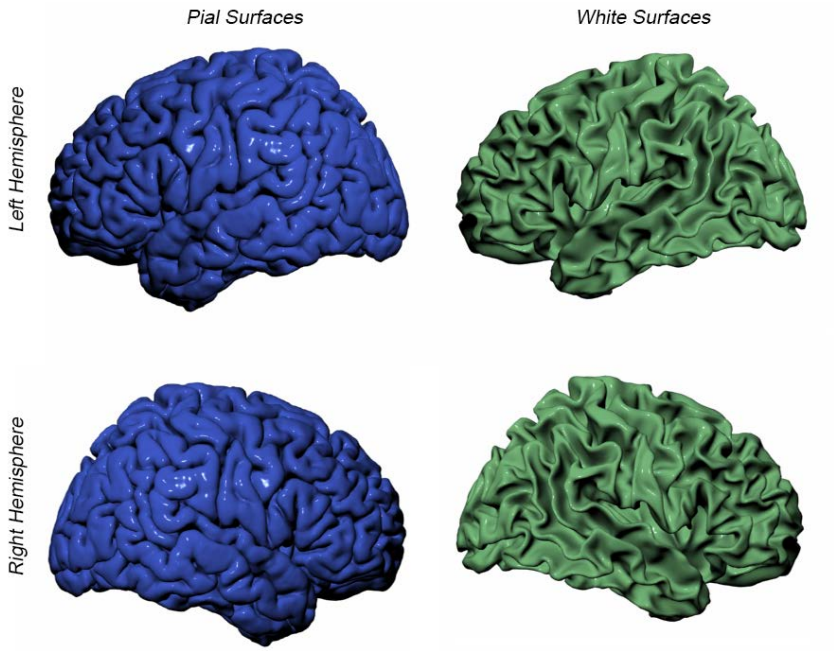

Figure 2.5: *Pial surface (left) and white surface (right).*

Apart from the cortical surfaces, two other surfaces can also be derived from the cortical surfaces: the *inflated surface* and the *hull surface*. The *inflated surface* (Figure 2.6A) is built by unfolding the cortical surface so no sulci are hidden behind a fold. In other words, it raises sulci to the surface for better visualization. The *hull surface* (Figure 2.6B) is similar to the pial surface but without the inner sulci. Covering the pial surface with a smooth envelope but not pushing it into the sulci generates it.

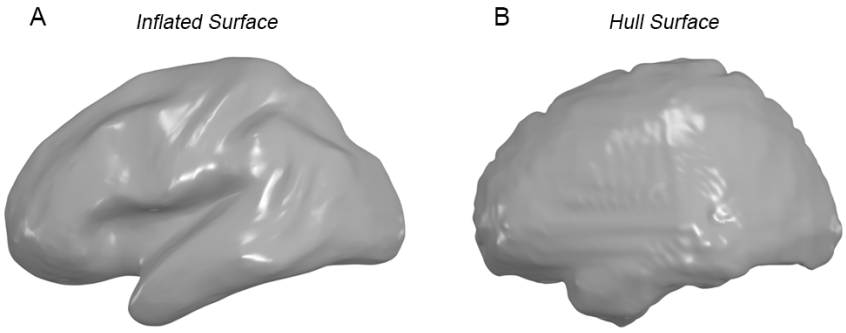

Figure 2.6: ***A)*** *Inflated surface.* ***B)*** *Hull surface.*

2.3. Morphometric biomarkers

A biomarker is a medical sign that can be measured with accuracy and reproducibility (Strimbu & Tavel, 2010). In the context of brain morphometry, it is a measurable indicator for monitoring a neurodegenerative disease or analyzing neurodevelopment. Therefore, their major goal is to improve early detection of neuronal

disorders and assess evolution of the disease. Its main advantage rises from the fact that biomarkers can be compared across different individuals and across different times. This Project will focus on the extraction of brain sulcal width, which can be used as a brain morphometric biomarker. Additionally, sulcal depth will also be calculated.

Both of these biomarkers belong to the group of *cortical* biomarkers, given that they are obtained from the previously explained cortical surfaces. Note that these surfaces are extracted from T1W-MRI images.

2.3.1 Cortical biomarkers

Cortical biomarkers (Figure 2.7) refer to quantitative measurements taken along the cortical surfaces. They can be taken both global and local, although only local are considered in this Project. The ones studied are:

***Cortical thickness** (CT)*: Cortical thickness at a given point refers to the distance between the inner boundary of the cortex and its outer boundary (Nam et al., 2015). It can also be explained as a measurement of the neuronal density that resides between the white and pial surfaces.

Area: Area at a given point of the mesh is defined as the average of the sum of the areas of all the triangles that the point belongs to.

***Local gyrification index** (LGI)*: it measures the quantity of cortex buried within the sulcal folds with respect to the amount of visible cortex (Schaer et al., 2012).

Curvature map: The curvature map saves the value of the curvature of each point of the cortical mesh. Curvature will be convex for points that belong to the gyri and concave for points from the sulci. Therefore, by looking at the curvature map a general ideal can be drawn on where sulci and gyri are located over the cortical surface.

Depth map: The depth map resembles the curvature map. However, the depth map saves the value of the depth of each point of the cortical mesh instead of the value of the curvature. Depth is defined as the distance between each point of the sulcal basin and its closest point in the gyral crown line.

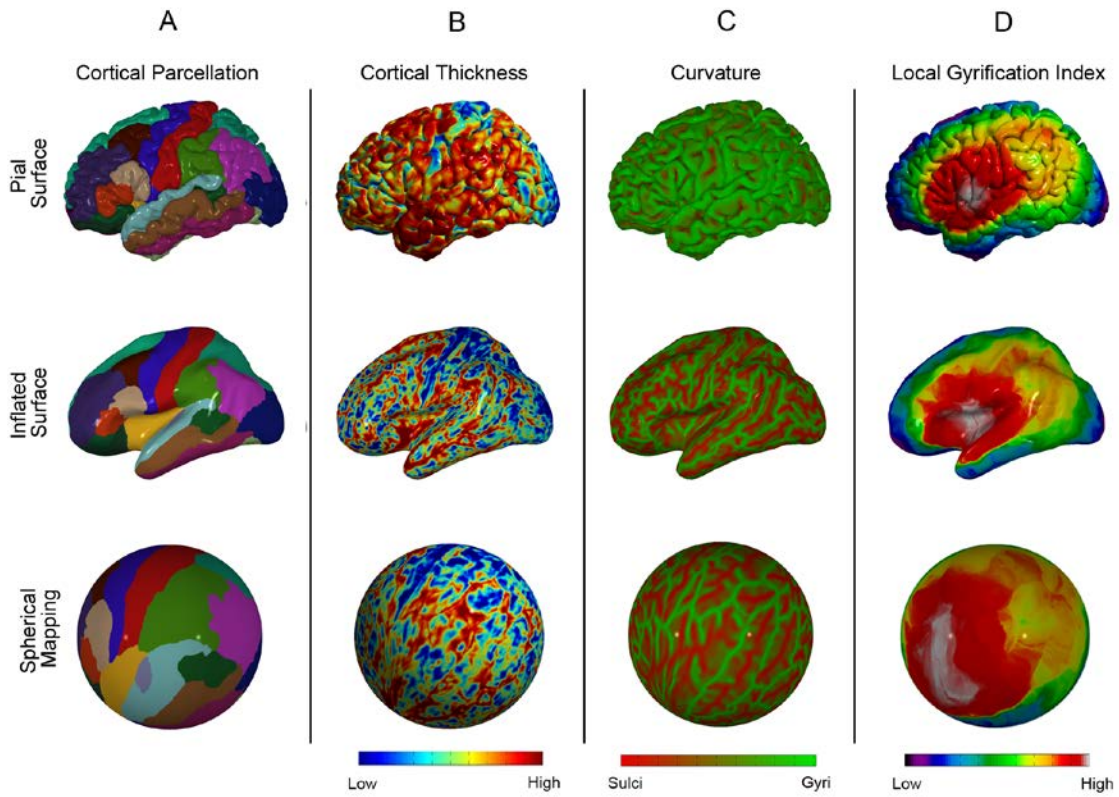

Figure 2.7: *Cortical biomarkers. Cortical parcellations (**A**), cortical thickness (**B**), curvature (**C**) and local gyrification index (**D**) maps on pial, inflated and spherical surfaces.* ***Note:*** *Inflated and spherical surfaces are used for better visualization.*

The curvature map will be employed, in this project, as input for sulcal lines, gyral crowns and sulcal width maps computation.

2.4. Previous work on sulcal width estimation

A more formal definition of sulcal width refers to it as the distance between two points of the pial surface (gray matter mesh) that belong to different sides of the sulcal basin. These two points should have a similar depth.

The calculation of a sulcal width map is important for the quantification of cerebral atrophy due to aging (J.-F. Mangin et al., 2010), brain disorders such as dementia (Jouvent et al., 2012) or neurodegenerative diseases (Pirttilä et al., 1993). Sulcal width also has an important application for the study of cognitive functions (Liu et al., 2011). However, not much investigation has been done in this field and there is barely any previous research.

A short review on algorithms proposed by different authors in the literature is introduced in the following section.

Method #1: Object Based Morphometry – Fold Opening (FO)

In 2010, (J.-F. Mangin et al., 2010) suggested the first approach for brain sulcal width calculation, also referred to as fold opening (FO), in which they calculated an indirect measurement of the width by dividing the total volume of CSF in the sulcus by the surface of a skeleton mesh that is previously constructed (see Figure 2.8 and expression (1)). This mesh runs parallel to the sulcal walls along the middle of the sulcal width covering the entire sulcal depth. It is built from the previous extraction of the cortex topography from a T1-weighted 3D MR image and its subsequent representation through an attributed relational graph (ARG) (J. Mangin et al., 1996). The graph is made up of nodes (gray matter and cerebrospinal fluid union's sub-patterns) and branches (mutual relations between the sub-patterns) either delimiting gyrus nodes or connecting skeleton nodes. Attributes from nodes and branches vary from area or orientation to depth of folds. Once the graph is constructed, the medial sulcal mesh is generated from the calculation of a 3D medial axis.

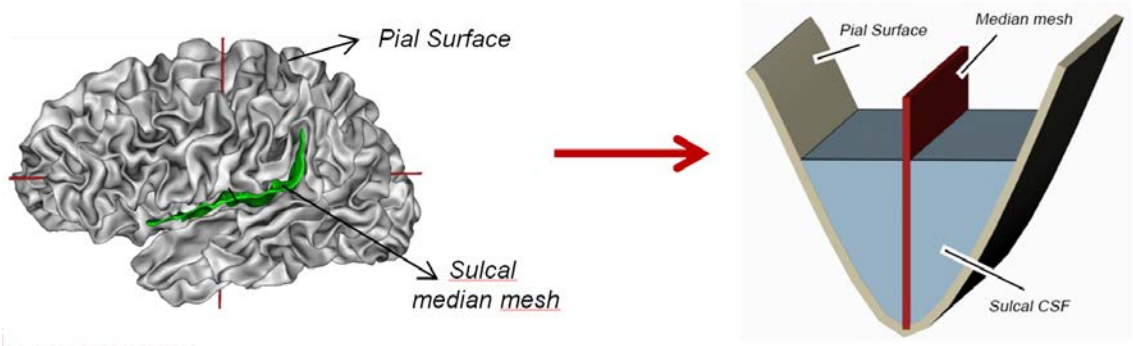

Figure 2.8: *Sulcus tridimensional diagram.*

In this case, sulcal width is defined as the average distance between gyral walls.

$$FO = \frac{V_{CSF}}{Amed.mesh} \quad (1)$$

The main issue of this algorithm rises from the fact that sulcal width calculation is an indirect measurement given as an average for the entire sulcus (region of interest). To calculate this volume it is assumed that the sulcus basin has a rectangular cubic shape. However, brain sulci has a variable topology and that assumption is an oversimplification of the problem. Another issue from this method is that the

measurements do not refer to points on the cortical surface, so cortical changes cannot be studied locally but instead they are only studied globally (for the entire sulcal basin). This is because the measurement is dependent on the construction of the medial mesh, in other words, from the method being object based.

Method #2: Object Based Morphometry – Sulcal Span (SS)

In 2012, (Kochunov et al., 2012) developed an improved tool for Brainvisa with the aim of estimating brain sulcal span so as to quantify cerebral changes linked to brain disorders. They proposed a method for its calculation in which a medial sulcal mesh is generated for each individual sulcus.

For each point in the medial mesh, two vectors are then traced along a normal direction to the medial wall up to their intersections with the gray matter mesh (see Figure 2.9). These vectors have to intersect on both sides of the sulcal basin; otherwise the other intersection point is rejected. Intersections within 4 mm from the adjacent sulci are also removed. With the remaining intersections, the Euclidean distance is calculated between the two intersections corresponding to a given point of the medial wall. The average between 500-5000 of these measurements is considered as the mean sulcal width.

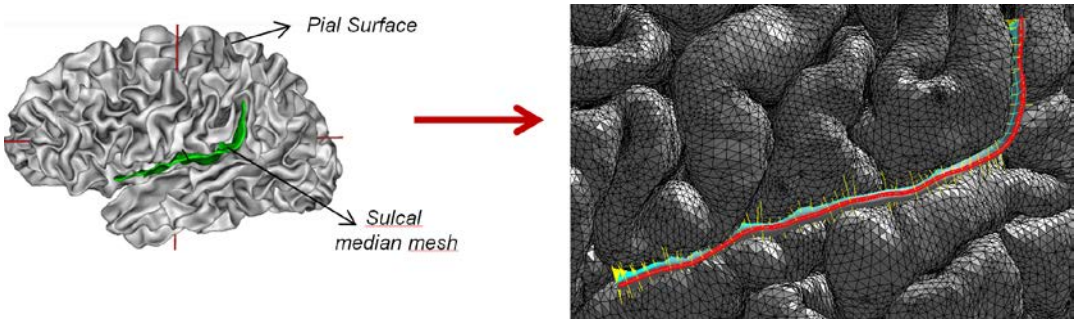

Figure 2.9: *Basic scheme for sulcal span calculation.* ***Note:*** *In yellow, the sulcal width vectors are displayed.*

This method has three main drawbacks. Firstly, sulcal width measurements do not refer to points on the cortical surface but to points from the medial wall, given that this method is also object based. Therefore, pointwise information for quantification of brain disorders is not optimal, since changes can only be studied globally. A width map with the span of each point of the cortical surface cannot be built. Secondly, this algorithm does not take into account the possibility of not having sulcus with a symmetric and homogeneous geometry. For example, the wall at one side can be larger

than at the other side. However, points without a pairing point at the opposite side along the same normal direction are rejected. Therefore, the sulcal width corresponding to these points on the taller side of the sulcus is not computed. This means that when the average is calculated, the result obtained is not accurate enough: some very important and probably larger distances that would modify the average are not being taken into account. Thirdly, it could happen that the sulcus is very folded, generating normal vectors intersections with gray matter at points that reside on adjacent sulci. This would lead to an erroneous measurement of the sulcal span at that point.

To sum up, it is clear that a new method for computing sulcal width from cortical surfaces must provide measurements that refer to each of the points of the cortical gray matter mesh (pial surface). Results can be compared with the ones obtained from the previous methods, but keeping in mind that they are not optimal. Therefore, since our approach is novel, there is no gold standard.

Chapter 3: Sulcal width maps computed over the human cortical surface

The main goal of the methodology developed in this Project is to build a vertexwise sulcal width and depth map. This map will provide local information about how this morphological properties change across the human brain cortex. For this reason, the generation of sulcal width and depth maps are expected to lead to a more profound understanding of neurodegenerative diseases, which was described in further details in Chapter 1.1.

The proposed method includes three main steps: 1) sulcal basin segmentation, sulcal lines and gyral crowns extraction, 2) depth map generation from previous sulcal basins surface and 3) sulcal width maps estimation. An overall workflow about the developed methodology can be observed in the following figure (see Figure 3.1).

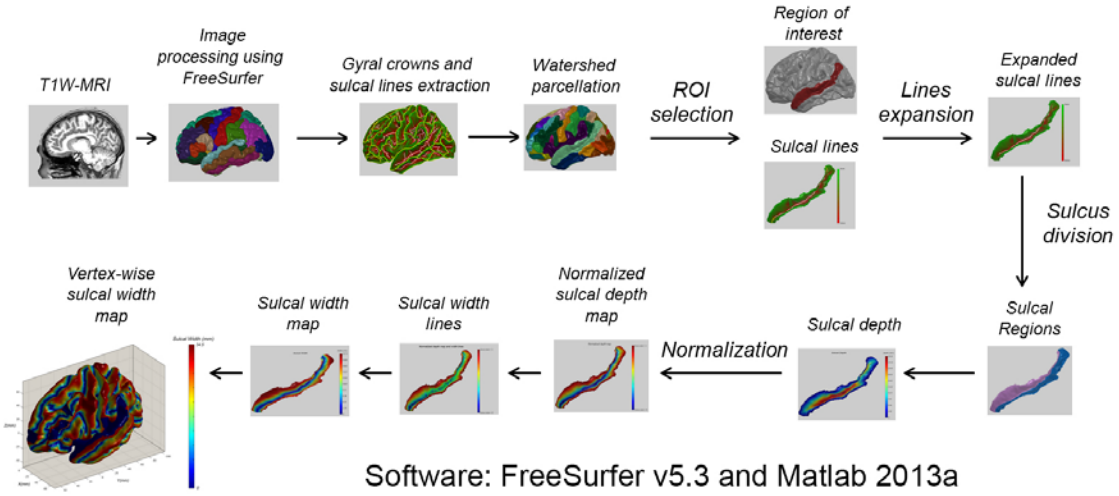

Figure 3.1: *Workflow of the developed methodology.*

The next diagram (Figure 3.2) represents a schematic view of the programming steps required to perform the image processing steps displayed in Figure 3.1. Screenshots of the developed matlab scripts are shown in Appendix A.

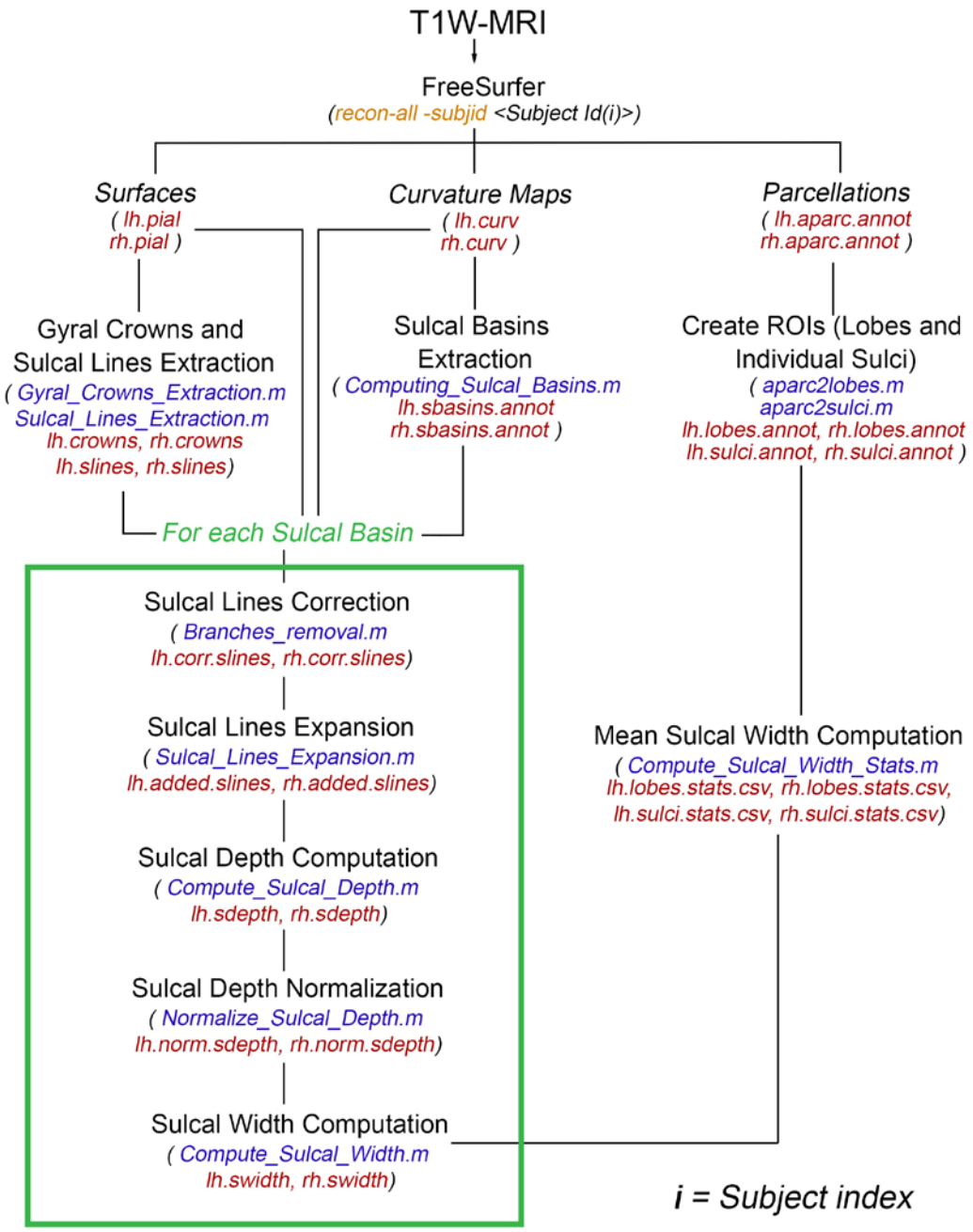

Figure 3.2: *Algorithm code workflow (**orange** = bash scripts, **green** = loop, **blue** = matlab functions and **red** = outputs).*

A 60 virtual machines cluster will be used to execute all computational methods. Each of these virtual machines is formed by a single core processor (2GHz or 2.6 GHz), 50 GB of storage capacity and 6 GB RAM. They also include the software packages for image processing needed in this work: Matlab (v2013), FreeSurfer (v5.3) and Brainvisa (v4.4).

3.1. Subjects sample and image acquisition

A total of eighty-five unrelated subjects obtained from the Human Connectome Project (HCP) database met the inclusion criteria for this Project. This data present a high quality in terms of resolution and contrast, which ensures an easier implementation and evaluation of the developed algorithms.

MRI scanning was performed using a 3T Siemens Skyra magnetic resonance scanner with a 32 channels head coil at Washington University. All subjects followed the same acquisition protocol, which comprises four different MRI modalities: resting-state fMRI (rfMRI), task fMRI (tfMRI), diffusion-weighted MRI (dwMRI) and structural MRI. However, only the last one was chosen for this work. Their scanning parameters can be seen in Table 3.1.

TYPE	T1w	T2w
Description	3D MPRAGE	3D T2-MPRAGE
TR (ms)	2400	3200
TE (ms)	2.14	565
TI (ms)	1000	
Flip Angle	8 deg	variable
FOV (mm)	224x224	224x224
Voxel Size	0.7 mm isometric	0.7 mm isometric
BW (Hz/Px)	210	744

Table 3.1: *Data and image acquisition specifications for the images used in this work. These data was obtained from http://humanconnectome.org/documentation/data-release/Q1_Release_Appendix_I.pdf.*

Further details about the acquisition protocol are described in (Van Essen et al., 2012).

3.2. Image processing

Brain mask extraction and intracranial volume assessment

A general processing stream was performed so as to obtain brain tissue segmentation images using a software package called SPM8 (Wellcome Trust Centre for Neuroimaging, London, UK; available at: http://www.fil.ion.ucl.ac.uk/spm) (Ashburner & Friston, 2005). Briefly, brain masks calculation was accomplished using

white matter (WM), gray matter (GM) and cerebrospinal fluid segmentations obtained from the VBM8 toolbox (available at: http://dbm.neuro.uni-jena.de/vbm) (Koutsouleris et al., 2012). This toolbox computes an algorithm that first gives a skull-stripped 'p0' image as a result. This image contains brain tissue divided into GM, WM and CSF. In order to correct possible brain segmentation errors this image was visually examined for each subject and skull was removed if necessary. This produced the final binary brain mask. Finally, to obtain the skull-stripped T1 the native T1-weighted image was multiplied by the binarized brain mask. Among all voxels in the binarized brain mask, those that were different from 0 were summed up in a total parameter referred to as intracranial volume (ICV). Note that the voxel size is 1x1x1 mm^3, the reason why only voxels different from zero were considered.

FreeSurfer Processing

Cortical thickness and gray matter regions' approximation for each subject was performed using the FreeSurfer package (version 5.3, http://surfer.nmr.mgh.harvard.edu), based on the anatomical T1-weighted image. In addition, cortical thickness, logical gyrification, area and curvature maps for the global brain were calculated from white (WM/GM boundary) and pial surfaces (GM/CSF boundary). These two surfaces were reconstructed following the methods described by (B Fischl et al., 1999; Bruce Fischl et al., 2002).

To sum up, FreeSurfer separates white matter, gray matter and subcortical structures to generate a triangular mesh of the topology and geometry of the pial surface (see Figure 3.3).

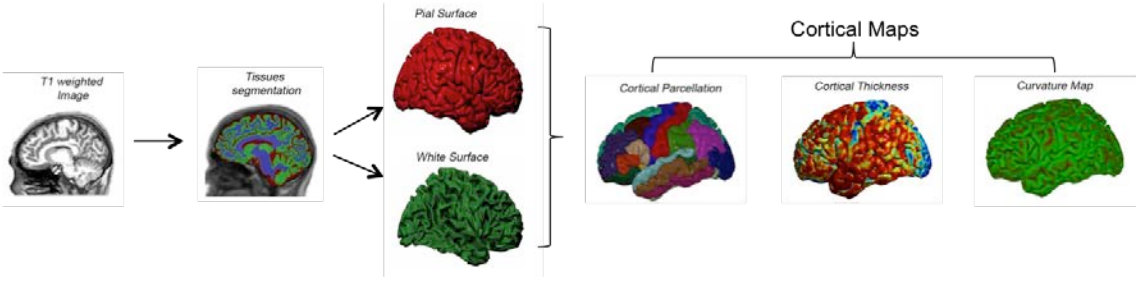

Figure 3.3: *FreeSurfer image processing workflow.*

3.3. Graph generation

The developed algorithm involves generating a non-directed weighted graph G_{basin}=(N,E,W) from a known surface, which is further explained in (Shattuck et al.,

2009) (see Figure 3.4). *N* is defined as the set of *nodes* (point in the 3D surface), *E* as the set of *edges* that compose the triangular mesh input surface (pair of indices of the vertices that form the connection) and *W* as the *edges weights*, which determines the degree of connection between the nodes of the edge. For this Project, the weight of each edge will be defined as the inverse of the average curvature of the two vertices that form the edge. The mathematical formulation that calculates the edge weight w_{ij} between two nodes *i* and *j*, whose curvature values are C_i for node *i* and C_{ij} for node *j* is:

$$w_{ij} = \frac{2}{C_i + C_j}$$

This weight definition allows for finding the path, between any two graph nodes, that minimizes the sum of weights along its edges using Dijkstra's algorithm (Dijkstra, 1959).

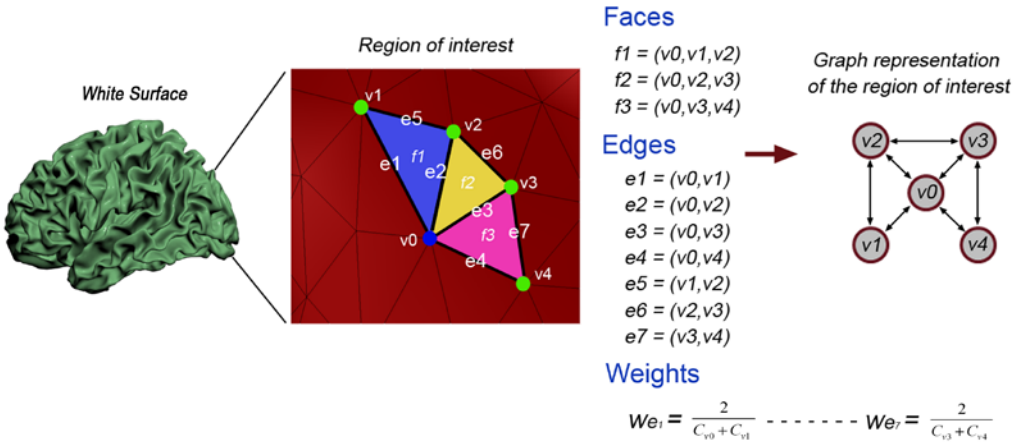

Figure 3.4: *Graph representation of a region of interest inside a sulcal structure formed by five vertices and three faces.*

The main advantage of using a graph representation of a surface mesh is that it allows for using all the properties, measures and algorithms that have been developed by the graph theory in order to characterize graphs structure and organization. One of the most employed indices in graphs characterization is the *node degree* (or *valency*). The node degree is the number of edges incident to a specific node and it allows for dividing the graph nodes into four main categories:

- *Isolated node*: A vertex with degree equal to zero is a vertex that is not an endpoint of any edge.

- *Leaf node* (also *pendant vertex*)**:** A vertex with degree equal to one. The sulcal line is a path (sequence of edges) connecting two leaves nodes.
- *Path node*: A vertex with degree equal to two means that this node is in the middle of a path between leaves or junction nodes.
- *Junction node*: A junction node (degree higher than two) is a vertex where two or more paths coming from leaves vertices intercept.

3.4. Sulcal basins segmentation and sulcal lines and gyral crowns extraction

The first step for the creation of sulcal width maps consists of the segmentation of the cortical surface to generate sulcal basins as well as the extraction of sulcal lines and gyral crowns. Sulcal basins are segmented prior to extraction of sulcal lines and crowns. These two processes are based on the use of a curvature map, which has values for each node of the cortical mesh according to its curvature.

Sulcal basins refer to the regions of points whose boundary are the imaginary lines between the sulci and the gyri. These points are positioned inside the inward-folded (concave) areas of the cortex. Therefore, they all have positive curvature indexes according to the FreeSurfer definition of curvature. In order to locate them on the surface, a threshold equal to zero is introduced in the curvature map: all values below zero are set to zero, while only positive values are kept as the sulcal basins.

Once sulcal basins are computed for the entire surface, sulcal lines are extracted for each of the sulcal basins. Firstly, a graph is constructed from the sulcal basin surface according to the methodology explained in the previous section (Figure 3.5A). Secondly, an step called *polygon breaking* is performed (Figure 3.5B). Polygon breaking is a procedure to eliminate the edge with the highest weight from each graph polygon. Thirdly, to detect and remove any graph cycles from the remaining graph its corresponding spanning tree graph is computed (Figure 3.5C). Fourthly, once we have obtained a tree-shaped graph, an iterative process, called *branch reduction*, is applied. The branch reduction step is the most important step, since it is responsible for obtaining the *sulcal basin skeleton* by eliminating edges from the graph structure (Figure 3.5D). A branch will be defined as the shortest path between a leaf node and its closest junction or leaf node. A branch path can be defined by the sequence of nodes or edges that forms the branch path.

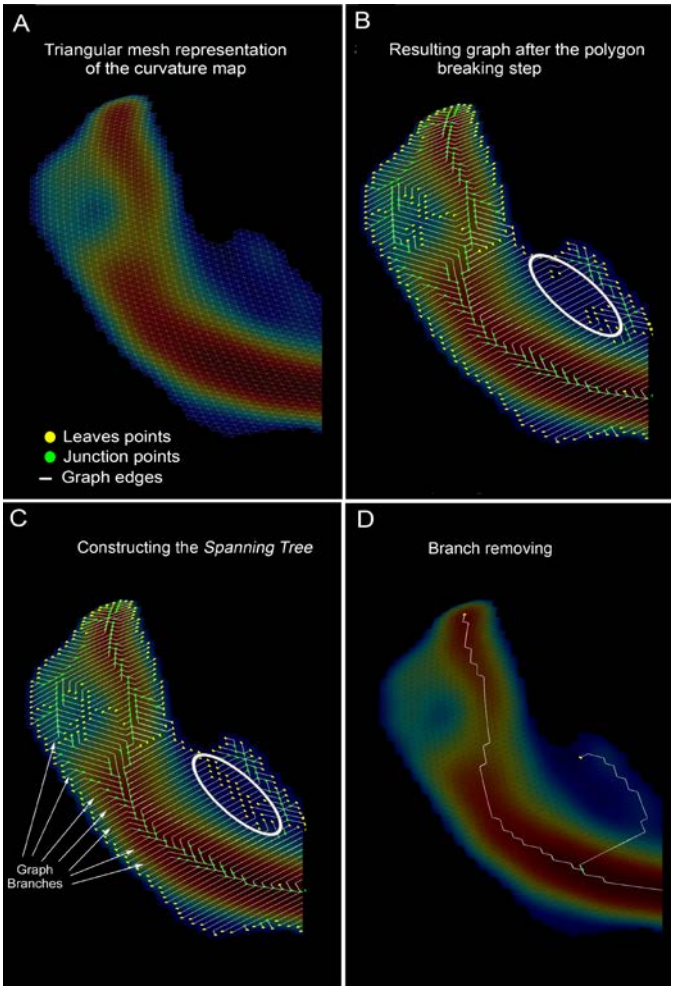

Figure 3.5: *Sulcal lines extraction steps.*

The gyral crowns extraction algorithm also starts from sulcal basins. First, the curvature values of the sulcal basins boundary points are compared to the curvature values of its unlabeled neighbors (see Figure 3.6B *(blue dots)*). If the curvature values of it unlabeled neighbors are higher than the curvature values of the labeled points, i.e. Figure 3.6C *(green dots)*, the boundary is moved to these neighboring points (Figure 3.6D). If the labeled neighbor points belong to different sulcal basins the growing point will be labeled with the tag present on the largest number of neighbors.

This procedure is repeated until every surface point is labeled. During this iterative process, each sulcal basin boundary grows only until the gyral maximum curvature points are reached due to the growth being curvature restricted (Figure 3.6). For this reason, it is impossible for the sulcal basins boundaries to move to an unlabeled

neighbor point with a lower curvature value. If all boundaries regions grow up to the maximum curvature points then these boundaries meet at the top of the gyri.

The number of watershed regions must be equal to the number of sulcal basins. Finally, based on this procedure, the gyral crowns are obtained simply by taking the boundaries between the regions created during the watershed parcellation.

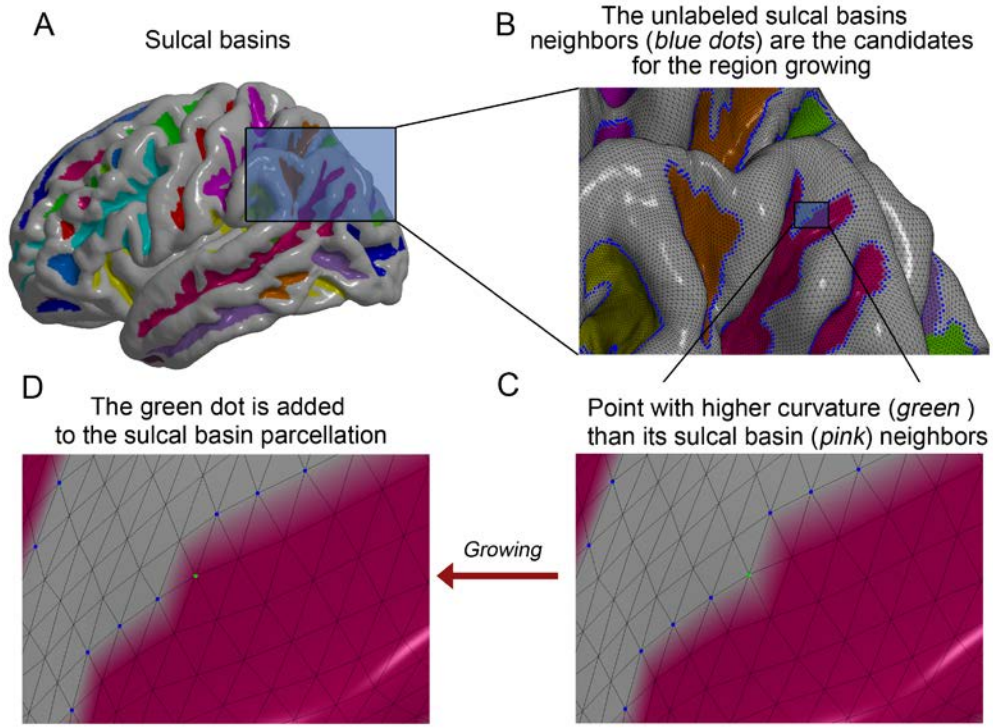

Figure 3.6: *Gyral crowns extraction algorithm. Sulcal basins grow during the curvature restricted watershed procedure.*

The methodology presented in this section for both gyral crowns and sulcal lines extraction was developed entirely at the Medical Imaging Laboratory located at Hospital General Universitario Gregorio Marañón. This methodology is currently pending on publication.

Sulcal basins are also labelled according to an anatomical protocol proposed by Klein (Klein & Tourville, 2012) which employs FreeSurfer cortical parcellation boundaries to label major brain sulci (see Appendix B). The following figure summarizes the sulcal basins computation as well as sulcal lines and gyral crowns extraction (Figure 3.7).

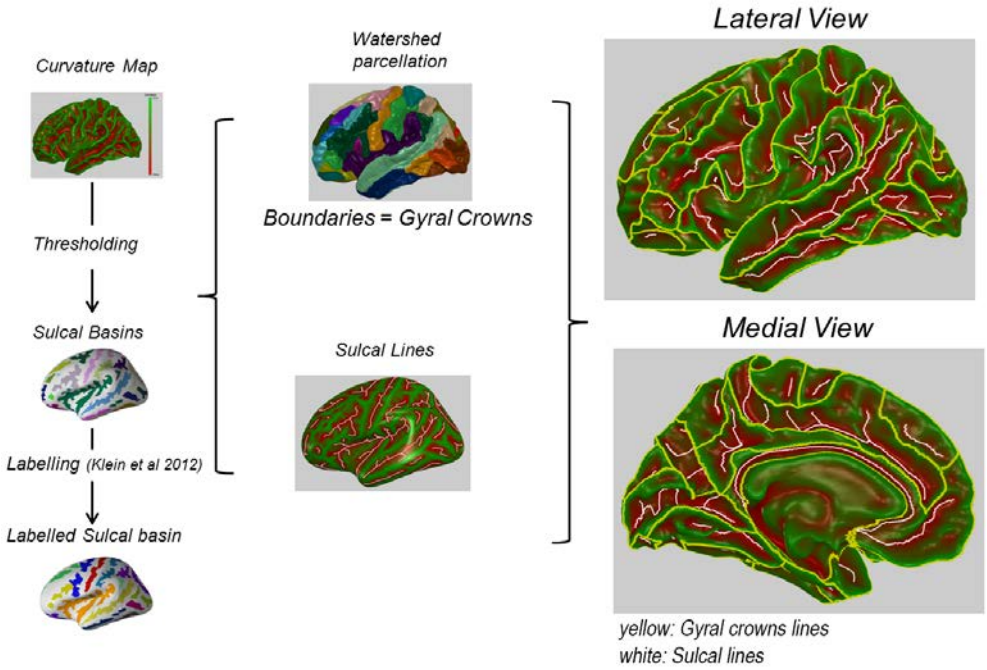

Figure 3.7: *Sulcal basin segmentation, sulcal lines and gyral crowns extraction workflow.*

3.5. Preliminary corrections

The extracted sulcal and gyral crowns lines, computed for each sulcal basin, present some topological errors that make them unsuitable for the requirements of this Project. On the one hand, some sulcal lines appear to have branches that do not correspond to the topology of the sulcus, although they belong to regions of maximum curvature (Figure 3.8A). Most of these branches follow the same pattern: they go up the wall of the sulcus and grow in towards the gyral crown.

In order to remove them, the normal vector of each vertex of the surface is computed. The angle (θ) between the normal vector of each leaf node (**P**) and the normal vector of its closest junction point (**Q)** is then calculated (see equation 2). If this angle is below 30º, then the branch is removed. The specified threshold was selected based on empiric evidence that this value removes the unwanted branches (see Figure 3.8).

$$\theta = \cos^{-1}\frac{P \cdot Q}{|P| \cdot |Q|} \qquad (2)$$

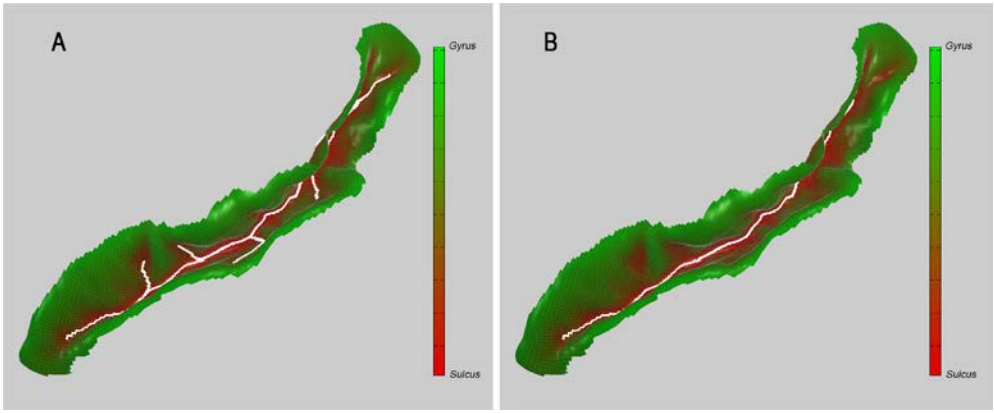

Figure 3.8: ***A)*** *Before branches removal and* ***B)*** *after branches removal.*

3.6. Sulcal lines expansion

Sulcal lines will be expanded, creating paths that run from each leaf node until their corresponding gyral crown point. The aim of this process is to divide the sulcal basin into different topological regions, so that width can be calculated between opposing regions. It involves two main stages: 1) creating temporal branches and 2) calculating the optimal sulcal lines expansion path.

Branches are created starting from the previously generated graph (see Chapter 3.3). For every triangle in the mesh, the edge with the lowest weight is removed. These newly created branches are not related to the topology of the sulcal region, thus they are not associated to the branches previously mentioned in Chapter 3.5. This step also requires finding the leaf nodes of the sulcal skeleton, since only branches ('temporal branches') that start at the leaf nodes are considered (see Figure 3.9).

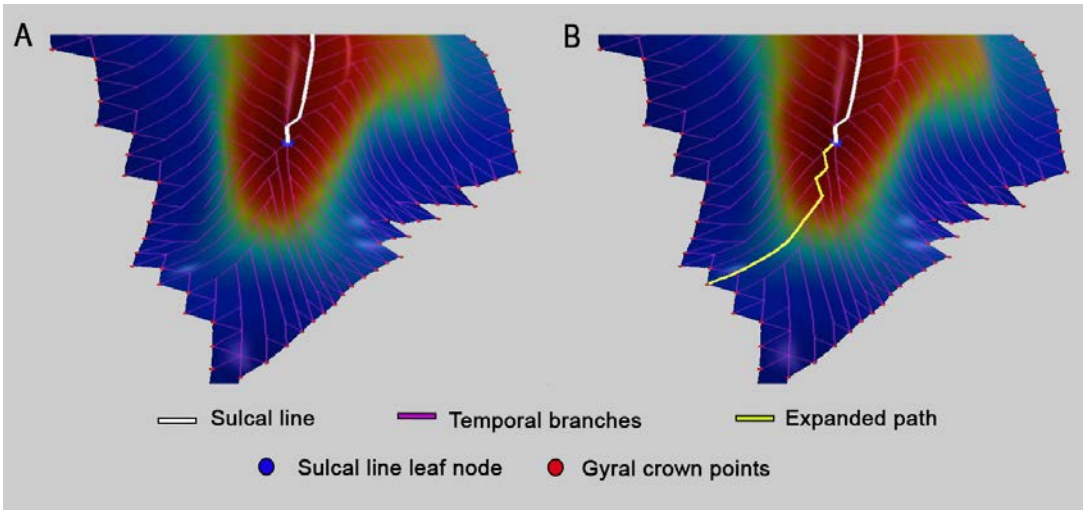

Figure 3.9: ***A)*** *Temporal branches.* ***B)*** *Temporal branches and expanded line path.*

These temporal branches are used to extract a subgraph from the previously created graph. In this case, the subgraph includes only those nodes that belong to the temporal branches. This subgraph along with the weights definition provides the starting point for the calculation of the sulcal line extension that accumulates the most curvature (minimizes the sum of weights throughout its edges) using Dijkstra's algorithm (Dijkstra, 1959). The shortest paths between each leaf node of the sulcal line (source node, *S*) and each point belonging to the gyral crown is computed using Dijkstra's algorithm implementation embedded in the function "*graphshortestpath*" distributed with MATLAB.

The selected path will be the one that accumulates the highest curvature in proportion to its length as well as grows straight (with no deviations) from the leaf node to the gyral crown. For this 'straight-growing' to happen, the path should be chosen so that it only goes through increasing levels. The level map is constructed setting the skeleton line as level 1 and its neighbors vertices set to be level 2. This is done for the rest of the sulcal basin until the gyral crown is reached (maximum level) (see Figure 3.10).

On the other hand, accumulated curvature along the path is divided by its geodesic length to avoid cases in which the accumulated curvature is very high, not because of the curvature itself but because of the length of the path.

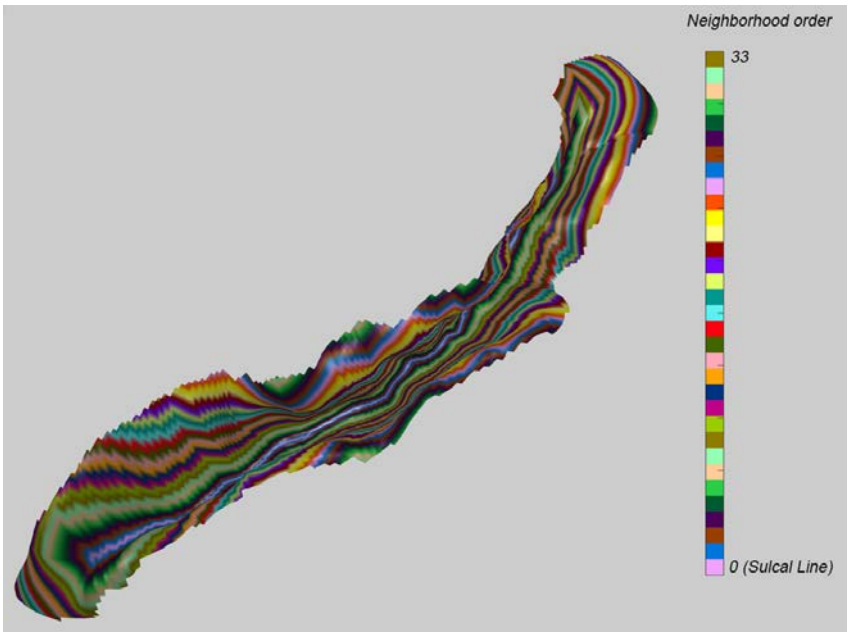

Figure 3.10: *Sulcal levels map.*

The calculation of the added line gives rise to a sulcal basin divided in regions according to anatomical topology (see Figure 3.11). The division is important for ensuring that the sulcal line remains as the path conformed by the points with the deepest depth values.

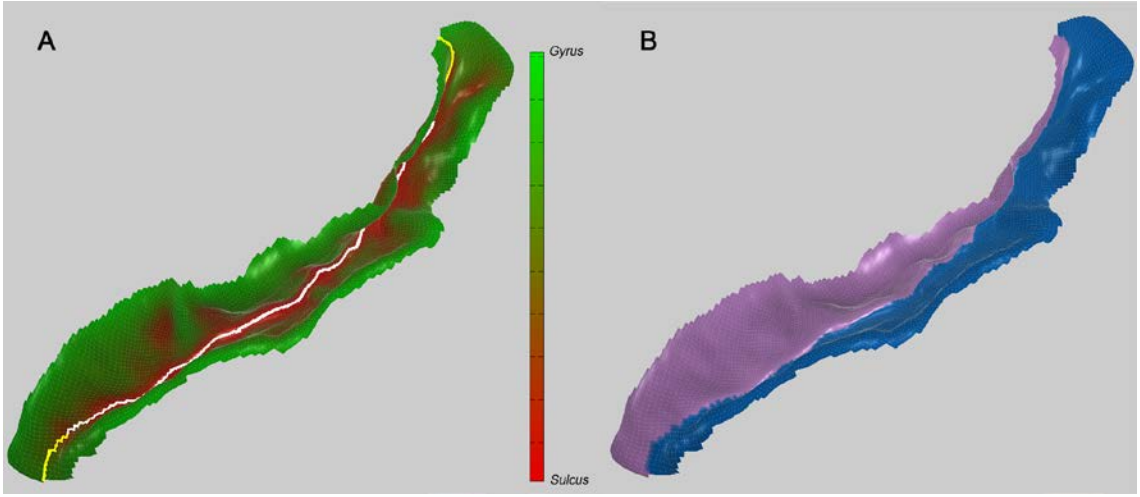

Figure 3.11: ***A)*** *Sulcal line expansion.* ***B)*** *Sulcal regions.*

3.7. Sulcal width calculation

In order to compute the vertexwise sulcal width map, a depth map is necessary. Different approaches have been considered for the definition of sulcal depth. The first and most obvious approach was to define sulcal depth as the Euclidean distance between points in the hull and pial surfaces. Euclidean distance works well for simple sulcal topologies like the one shown in Figure 3.12A, since points that belong to the sulcal line will have higher Euclidean depth than any other point in the pial surface. However, if the topology of the sulcus is more complex (see Figure 3.12B), Euclidean distance does not do a good job. As can be observed in Figure 3.12B, point C, which belongs to the sulcal line, has lower euclidean depth compared to the euclidean depth of point D, which is in the middle of the gyral bank. This measurement is therefore erroneous, given that point C belongs to the sulcal fundus, which contains the points of the sulcus with the highest depth. To overcome this problem, the geodesic distance was considered. Geodesic distance is defined as the length of the shortest path connecting two nodes, that goes throughout the surface. However, this distance still does not solve the problem of complex topologies. As seen in Figure 3.12C, a point D has a higher geodesic depth than point C, which forms part of the sulcal fundus. In order to be able to measure depth based on geodesic distances, sulcal basins need to be divided into

different regions to such that the sulcal line always runs along the path that contains the highest depth points. This is ensured if the sulcal depth map is computed individually for each topological region obtained in the previous step (Figure 3.11B).

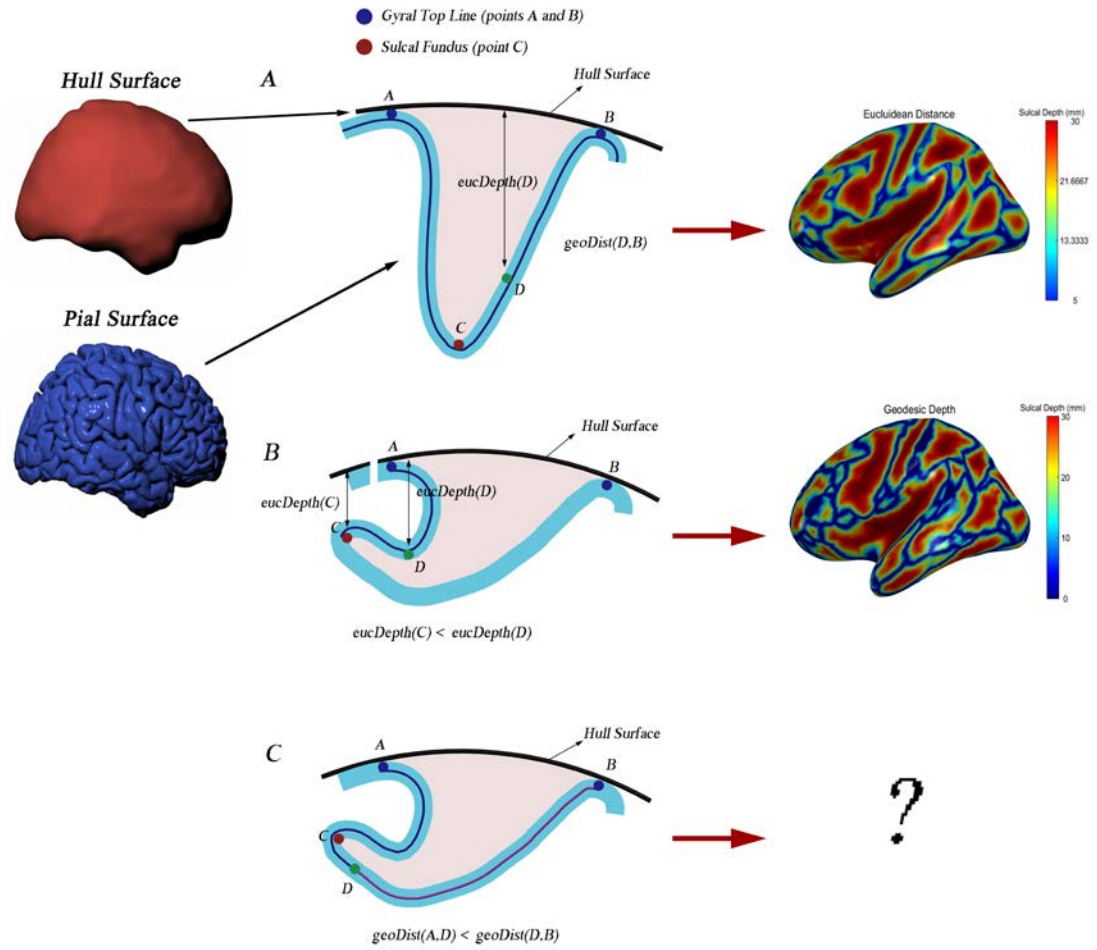

Figure 3.12: *Sulcal depth definitions.* ***A)*** *Euclidean distance.* ***B)*** *Geodesic distance.* ***C)*** *Proposed sulcal depth definition.*

Geodesic sulcal depth is then computed individually for each sulcal region (Figure 3.11B and Figure 3.13).

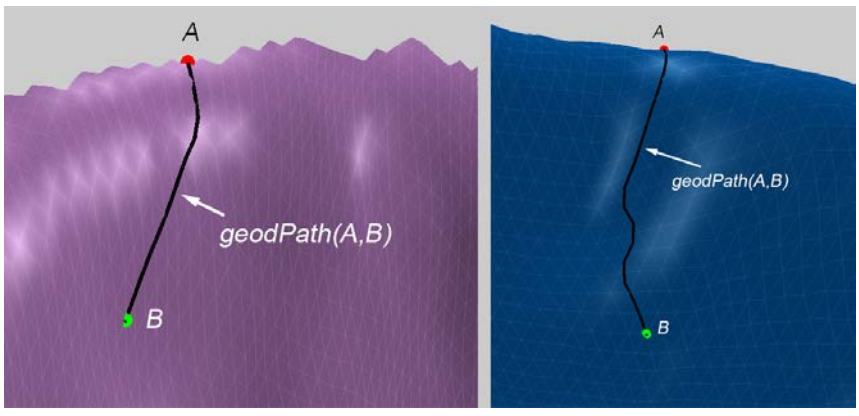

Figure 3.13: *Sulcal depth calculation for each individual region.*

These independent maps are then joined together to generate a vertexwise sulcal depth map. As can be observed in Figure 3.14, discontinuities appeared around the sulcal line: higher depth values are given for the larger gyral bank in comparison to depth values of the opposite and shorter gyral bank.

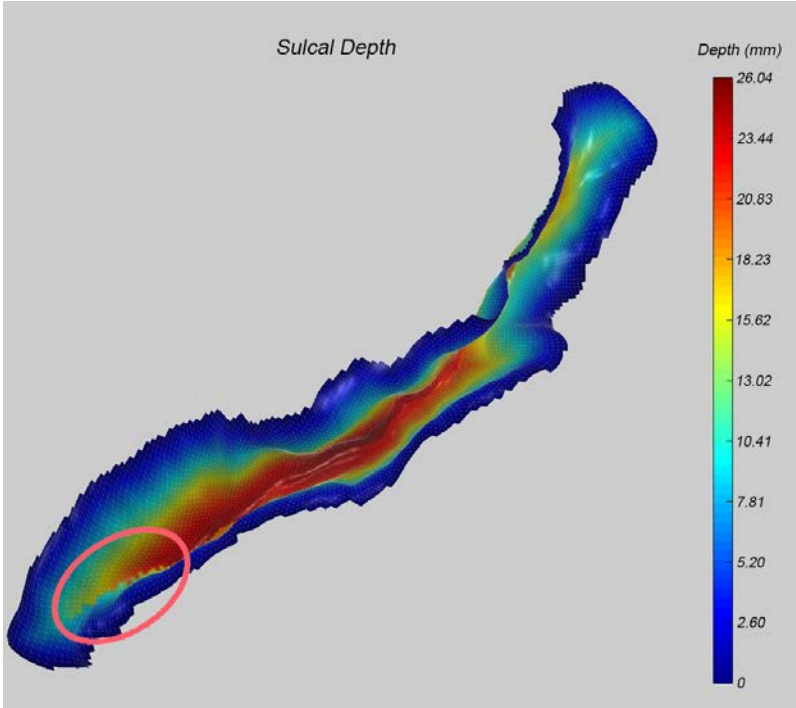

Figure 3.14: *Sulcal depth map.*

This map must be modified through a normalization step with the goal of eliminating these discontinuities around the sulcal line. The main idea of the normalization is to set to 1 the depth of all points belonging to the sulcal line and set to 0 the depth of gyral crown points. Points within the sulcus will present values between 0 and 1. This depth normalization is accomplished by applying the following formula (see Figure 3.15):

$$normgeodDist(BC) = 1 - \frac{geodDist(BC)}{geodDist(BC) + geodDist(AC)}$$

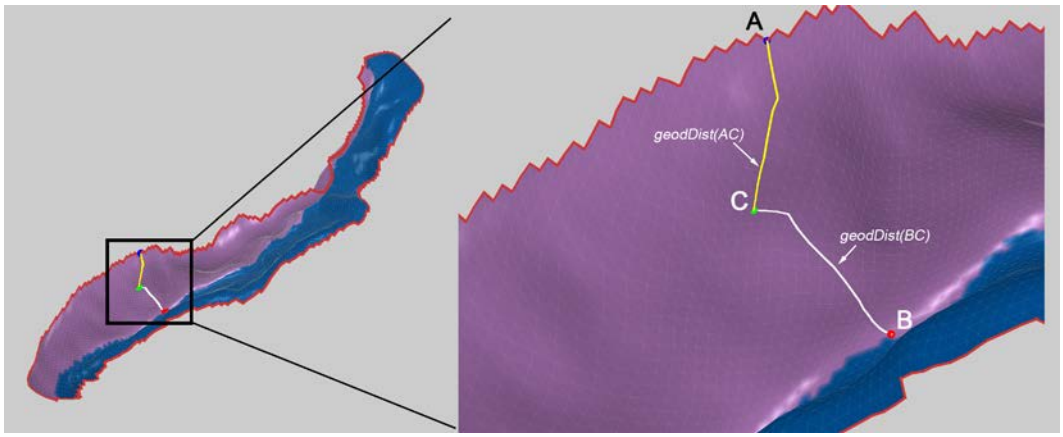

Figure 3.15: *Normalization scheme for one sulcal region (left). Zoom of the selected region of interest (right).*

Point *C* refers to any point within the sulcal basin, point *B* and point *A* are its closest points, measured in geodesic distance, that belong to the sulcal line and gyral crown respectively. This normalization is calculated as the quotient between the geodesic distance from point *C* to point *A* and the sum of the geodesic distances from point *C* to both point *A* and point *B*, as observed in Figure 3.15. This quotient is then subtracted from 1, to ensure that the maximum depth corresponds to the sulcal line. For example, if point *B* belongs to the sulcal line, the numerator of the quotient is zero, so that the normalized sulcal depth of this point is 1. The generated normalized sulcal depth map is shown in Figure 3.16.

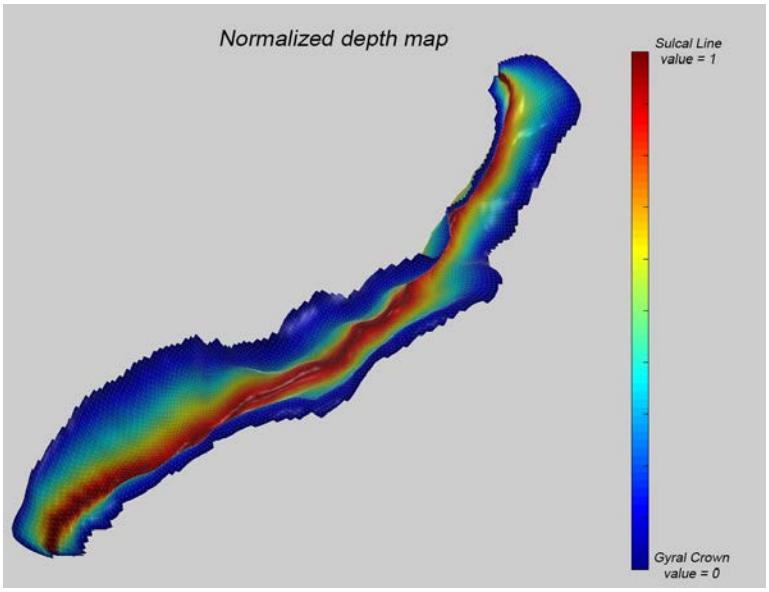

Figure 3.16: *Normalized depth map.*

Once normalization is performed, vertices belonging to opposite sulcal regions, within the same range of normalized depth and minimum euclidean distance between them are paired (Figure 3.17A). Each sulcal point has a paired vertex on another topological region of the sulcal basin which allows for computing a vertexwise sulcal width map for the whole mesh (Figure 3.17B).

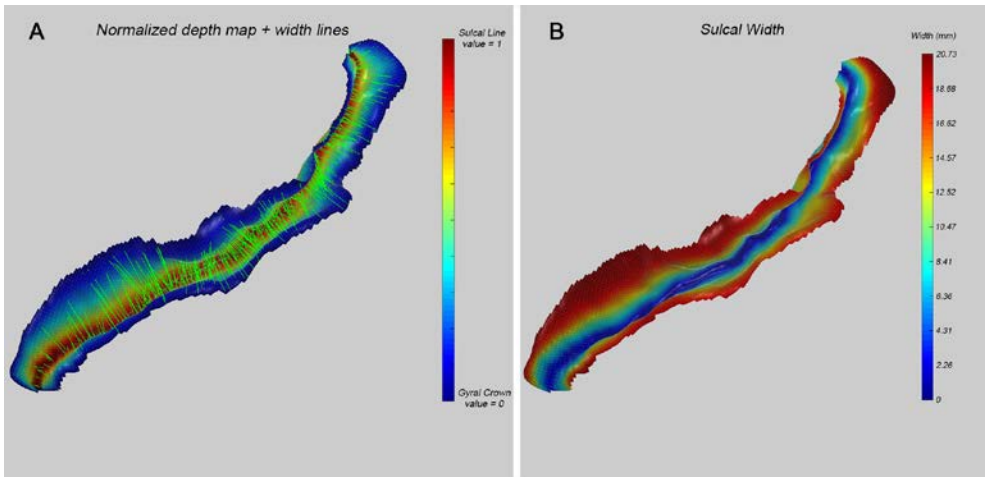

Figure 3.17: ***A)*** *Pairs of closest vertices with similar normalized depth.* ***B)*** *Vertexwise sulcal width map.*

Applying all these processing steps to each individual sulcal basin (see Figure 3.7), a sulcal width map for the whole brain cortex is obtained (see Figure 3.18).

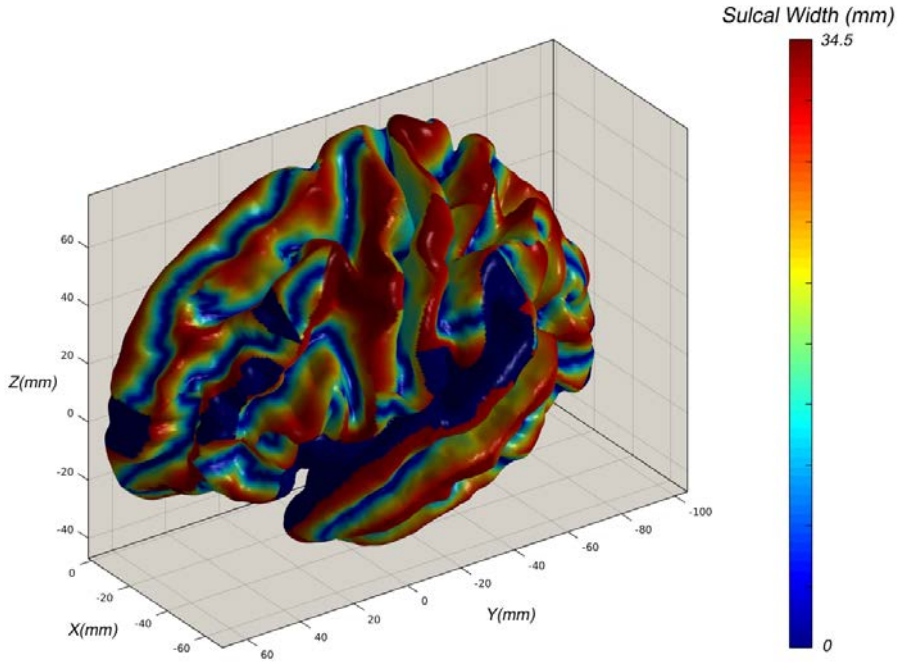

Figure 3.18: *Vertexwise sulcal width map of the entire cortical surface.*

Chapter 4: Results and discussion

The main objective of this chapter is to compare the sulcal width measurements produced by the developed methodology (SleSA-SW) to those obtained from both previous methods: (1) Object Based Morphometry- Fold opening (OBM-FO) (J.-F. Mangin et al., 2010) and and (2) Object Based Morphometry- Sulcal span (OBM-SS) (Kochunov et al., 2012).

As was mentioned before, object-based algorithms provide an average sulcal width for an apriori specified region of interest. Therefore, the vertex-wise sulcal width measurements produced by our method (SleSA-SW) need to be averaged in order to be comparable to the object-based methods (OBM-FO and OBM-SS).

For the first comparison the sulcal width is averaged over each brain lobe (frontal, occipital, parietal and temporal) and for the second comparison five major sulci were selected as a apriori regions of interest (central sulcus, cingulate sulcus, parieto-occipital sulcus, calcarine fissure and superior temporal sulcus) and the sulcal width was averaged over each of these sulci.

Two different statistical analysis are performed. First, a Student's t-test to test for differences in sulcal width measurements between SleSA-SW and the other two approaches (OBM-FO and OBM-SS). Second, a correlation and regression analysis to detect and quantify the relationship between sulcal width measurments from SleSA-SW and the object-based methods.

4.1. Student's t-test results

The Student's t-test is a common technique used for studying the difference between sample means. Two data samples are compared to give a statistic (t), a probability value (p) and an effect size value (d). The mathematical expression for the t-test is given by the following equation, where $\overline{x_1}$ and $\overline{x_2}$ are the means for the two samples, s_1^2 and s_2^2 are the variances of the two samples and n_1 and n_2 are the number of measurements in each sample:

$$t = \frac{|\overline{x_1} - \overline{x_2}|}{\sqrt{\frac{s_1^2}{n_1} + \frac{s_2^2}{n_2}}}$$

In this project, sample 2 will always be the proposed method SleSA and sample 1 will be either OBM-FO or OBM-SS. If both sets of samples are similar, the value of *t* will be small (close to zero). However, if they do not coincide, the value of *t* will increase. The larger the *t*, the greater the confidence that there is a difference. For the value of *t* to be significant, the p-value must be below 0.05. If *t* is large and widths are not widely spread out, the effect size will be large (above 0.8).

In the following figure and tables (Figure 4.1, Table 4.1 and Table 4.2), differences in lobar mean sulcal width are displayed.

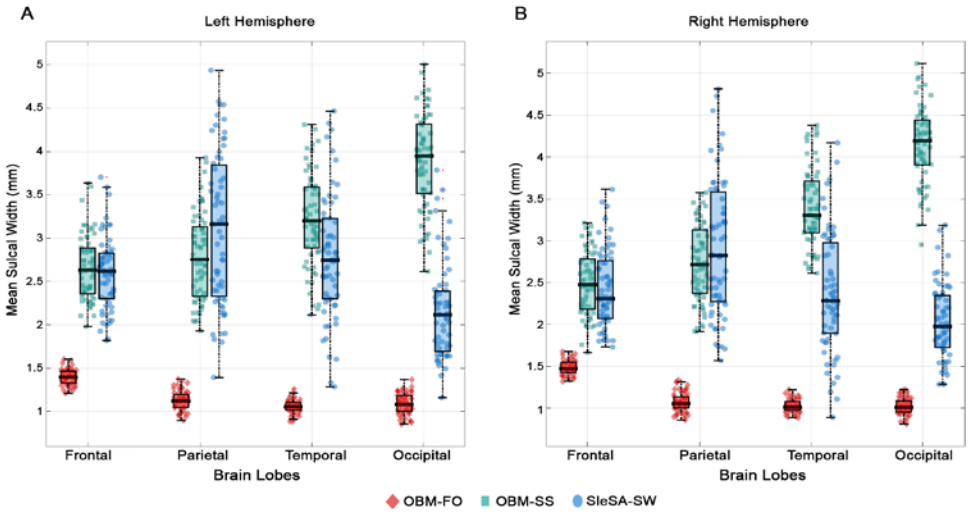

Figure 4.1: *Lobes sulcal width mean differences between the proposed method SleSA (**blue**) and two other methods: OBM-FO (**red**) and OBM-SS (**green**) for **A)** Left hemisphere and **B)** Right hemisphere.*

	Left Hemisphere				Right Hemisphere			
BRAIN LOBES	**Mean[1] (Std)**	**Mean[2] (Std)**	**t (p)**	**d**	**Mean[1] (Std)**	**Mean[2] (Std)**	**t (p)**	**d**
Frontal	1.34 (0.09)	2.60 (2.41)	-22.83 (1.85e-32)	-2.83	1.48 (0.08)	2.42 (0.45)	-17.03 (1.80e-25)	-2.11
Parietal	1.13 (0.11)	3.11 (0.86)	-18.54 (2.01e-27)	-2.30	1.07 (0.11)	2.92 (0.80)	-18.12 (6.83e-27)	-2.25
Temporal	1.06 (0.07)	2.79 (0.70)	-19.48 (1.35e-28)	-2.42	1.03 (0.08)	2.37 (0.71)	-15.39 (3.35e-23)	-1.91
Occipital	1.09 (0.12)	2.16 (0.56)	-14.94 (1.54e-22)	-1.85	1.02 (0.09)	2.03 (0.44)	-18.52 (2.10e-27)	-2.30

[1] Means Object Based Morphometry Fold Opening(OBM-FO)
[2] Means Sulcal Lines Extraction Algorithm Sulcal Width (SleSA-SW)

Table 4.1: *Lobes t-test results for OBM-FO vs SleSA-SW comparison.*

	Left Hemisphere				Right Hemisphere			
BRAIN LOBES	**Mean[1] (Std)**	**Mean[2] (Std)**	**t (p)**	**d**	**Mean[1] (Std)**	**Mean[2] (Std)**	**t (p)**	**d**
Frontal	2.66 (0.37)	2.60 (2.41)	0.86 (0.40)	0.11	2.49 (0.37)	2.42 (0.45)	0.92 (0.36)	0.11
Parietal	2.79 (0.50)	3.11 (0.86)	-2.73 (0.01)	-0.34	2.73 (0.46)	2.92 (0.80)	-1.62 (0.11)	-0.20
Temporal	3.21 (0.53)	2.79 (0.70)	3.98 (e-4)	0.50	3.39 (0.48)	2.37 (0.71)	8.76 (1.47e-12)	1.09
Occipital	3.89 (0.54)	2.16 (0.56)	17.32 (7.55e-26)	2.15	4.14 (0.45)	2.03 (0.44)	23.74 (1.93e-33)	2.95

[1] Means Object Based Morphometry Fold Opening(OBM-SS)
[2] Means Sulcal Lines Extraction Algorithm Sulcal Width (SleSA-SW)

Table 4.2: *Lobes t-test results for OBM-SS vs SleSA-SW comparison.*

From Figure 4.1, Table 4.1 and Table 4.2 it can be observed that the differences in sulcal width between SleSA-SW and OBM-SS (absolute $t < 8$, except occipital lobe) are lower than the differences between SleSA-SW and OBM-FO width values (absolute $t > 14$).

This lower difference could be related to the fact that in both cases the sulcal width estimation is computed based on the true euclidean distance between sulcal walls. The difference is higher for the occipital lobe because sulcal width calculation highly depends on sulcal lines extraction which may fail in the occipital cortex. Cortical surface reconstruction is known to be challenging in occipital brain regions and thus affects curvature indexes in that region. Sulcal line extraction strongly depends on curvature indexes which may explain the poor results obtained for this lobe.

It must be noted that a vast majority of the evaluated results show strength of evidence against the null hypothesis which states that there is no mean difference between the methods. Apart from this, the estimated strength of the two data samples is also meaningfully large because the effect sizes are mostly above 0.8. The only cases in which the null hypothesis was not rejected was for the frontal lobe in both hemispheres (p-values >0.05).

The same analysis is performed for brain sulci and the results are displayed in figure Figure 4.2 and summarized in tables (Table 4.3 and Table 4.4).

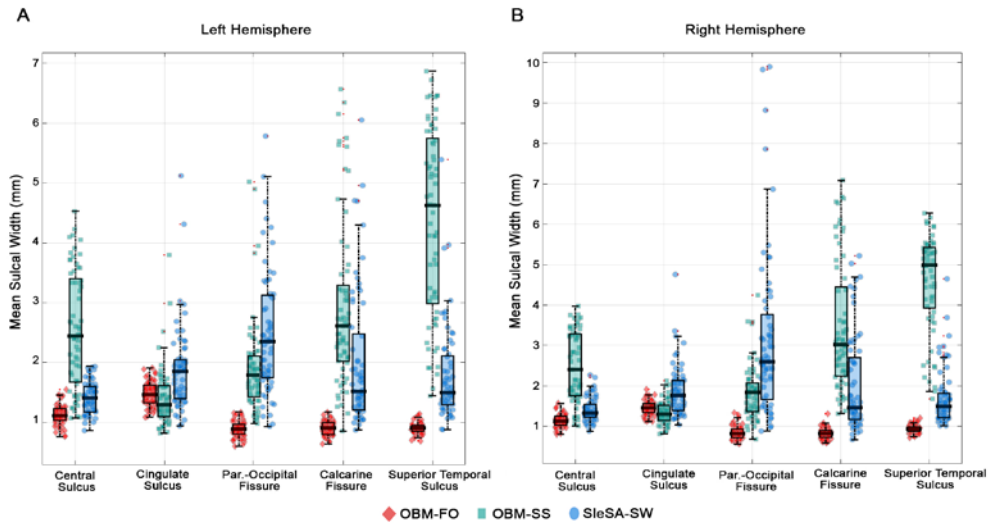

Figure 4.2: *Sulci sulcal width mean differences between the proposed method SleSA (**blue**) and two other methods: OBM-FO (**red**) and OBM-SS (**green**) for **A)** Left hemisphere and **B)** Right hemisphere.*

	Left Hemisphere				Right Hemisphere			
BRAIN SULCI	**Mean[1] (Std)**	**Mean[2] (Std)**	**t (p)**	**D**	**Mean[1] (Std)**	**Mean[2] (Std)**	**t (p)**	**d**
Central	1.12 (0.155)	1.41 (0.26)	-10.33 (2.87e-15)	-1.28	1.13 (0.14)	1.38 (0.25)	-9.691 (3.57e-14)	-1.20
Cingulate	1.47 (0.20)	1.78 (0.48)	-4.52 (2.75e-05)	-0.56	1.45 (0.16)	1.82 (0.52)	-5.223 (2.03e-06)	-0.65
Parieto-Occipital	0.89 (0.13)	2.39 (0.88)	-13.43 (2.73e-20)	-1.67	0.83 (0.13)	2.84 (1.42)	-11.24 (8.41e-17)	-1.40
Calcarine	0.89 (0.12)	1.90 (0.95)	-8.30 (9.26e-12)	-1.03	0.82 (0.12)	1.98 (1.13)	-8.419 (5.88e-12)	-1.04
Sup. Temporal	0.90 (0.08)	1.66 (0.53)	-11.68 (1.60e-17)	-1.5	0.94 (0.09)	1.62 (0.54)	-10.56 (1.17e-15)	-1.31

[1] Means Object Based Morphometry Fold Opening (OBM-FO)
[2] Means Sulcal Lines Extraction Algorithm Sulcal Width (SleSA-SW)

Table 4.3: *t-test results for OBM-FO vs SleSA-SW comparison in five major sulci for both hemispheres.*

	Left Hemisphere				Right Hemisphere			
BRAIN SULCI	**Mean[1] (Std)**	**Mean[2] (Std)**	**t (p)**	**d**	**Mean[1] (Std)**	**Mean[2] (Std)**	**t (p)**	**d**
Central	2.54 (0.98)	1.41 (0.26)	8.44 (5.39e-12)	1.05	2.49 (0.86)	1.38 (0.25)	9.82 (2.12e-14)	1.22
Cingulate	1.34 (0.34)	1.78 (0.48)	-6.52 (1.29e-08)	-0.80	1.33 (0.27)	1.82 (0.52)	-7.25 (6.84e-10)	-0.90
Parieto-Occipital	1.78 (0.50)	2.39 (0.88)	-5.15 (2.70e-06)	-0.64	1.75 (0.51)	2.84 (1.42)	-5.89 (1.58e-07)	-0.73
Calcarine	2.87 (1.33)	1.90 (0.95)	4.53 (2.63e-05)	0.56	3.45 (1.59)	1.98 (1.13)	6.14 (5.84e-08)	0.76
Sup. Temporal	4.35 (1.57)	1.66 (0.53)	13.51 (2.06e-20)	1.68	4.58 (1.20)	1.62 (0.54)	17.42 (5.47e-26)	2.16

[1] Means Object Based Morphometry Fold Opening(OBM-SS)
[2] Means Sulcal Lines Extraction Algorithm Sulcal Width (SleSA-SW)

Table 4.4: *t-test results for OBM-SS vs SleSA-SW comparison in five major sulci for both hemispheres.*

When performing the comparisons for the individual sulci, results are slightly different than for the lobes. The mean differences are lower (smaller *t* values) when comparing OBM-SS and SleSA-SW compared to SleSA-SW vs OBM-FO. This is due to the fact that sulcal topology varies considerably between subjects. In the case of brain lobes, mean differences vary less because pointwise sulcal width values are averaged over the entire lobe spanning thousands of vertices.

All the selected sulcal regions present significant differences between SleSA-SW and both OBM-FO and OBM-SS (all p-values <0.05).

Caution is warranted when interpreting the results of this comparison of methods. Comparisons were performed with two methods that do not compute pointwise sulcal width like the developed methodology. Thus the accuracy of these methods cannot be compared to the developed method. In addition, no gold standard sulcal width maps or other vertexwise approaches are available in the literature, which further complicates interpretation of the comparisons.

In general, sulcal width values measured using OBM-SS as well as SleSA-SW are higher than fold opening values.

4.2. Correlation and regression analysis

The main idea of using correlation analysis is to study how individual sulcal width measurements computed with the proposed method relate to individual sulcal width measurements computed with the other methods. The regression line is used to quantify the relationship between the different sulcal width measurements. All the analyses were performed for the same regions of interest (four lobes and five major sulci) .

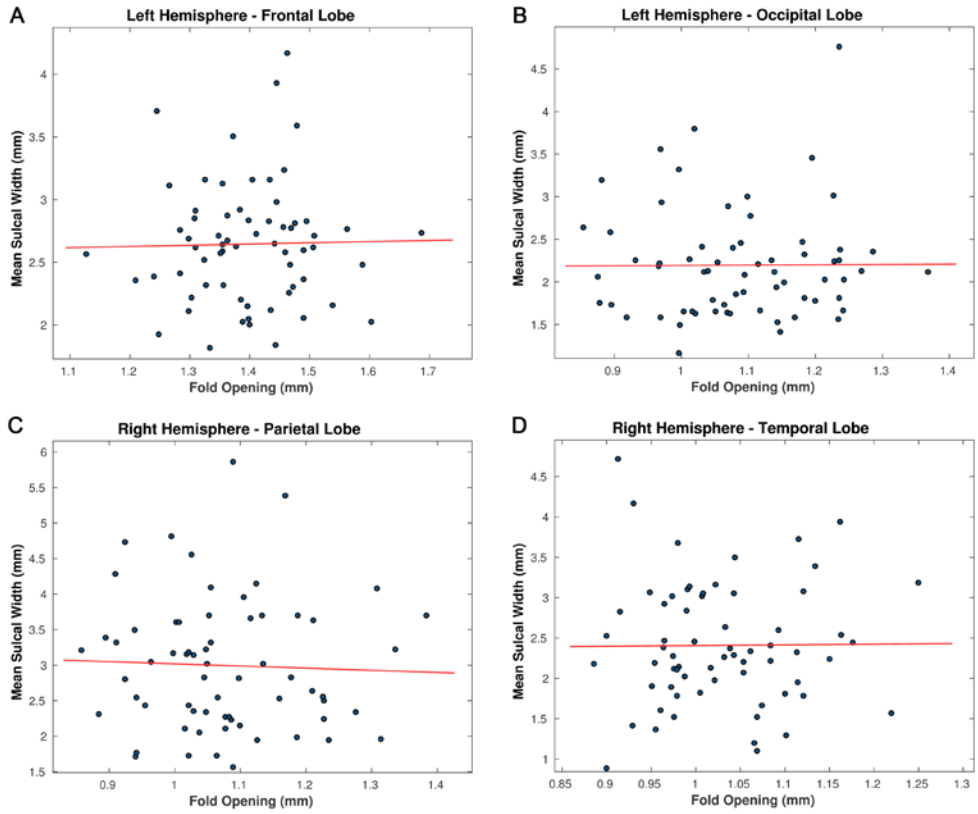

Figure 4.3: *Relationship of sulcal width values computed for both methods SleSA-SW (y axis) and OBM-FO (x axis). The regression line is displayed in* ***red****.*

	Correlation		Regression	
BRAIN LOBE	**r**	**p-value**	**Slope**	**Intercept**
Frontal Left	0.019	0.019	0.019	0.019
Frontal Right	0.027	0.027	0.027	0.027
Parietal Left	0.003	0.003	0.003	0.003
Parietal Right	-0.038	-0.038	-0.038	-0.038
Temporal Left	-0.193	-0.193	-0.193	-0.193
Temporal Right	0.008	0.008	0.008	0.008
Occipital Left	0.007	0.007	0.007	0.007
Occipital Right	0.026	0.026	0.026	0.026

Table 4.5: *OBM-FO vs. SleSA-SW correlation and regression results for brain lobes.*

The information provided by the previous image (Figure 4.3) and table (Table 4.5) establishes that there is no (linear) relationship between lobar OBM-FO and SleSA-SW values. The correlation coefficients *(r)* and regression slopes are close to zero, which also indicates no connection between sulcal width and fold opening metrics. As can be observed in Figure 4.3D, sulcal width values range up to 4 mm (if outliers are

discarded) while fold opening maximum is 1.4 mm. This mean difference coincides with the results obtained in previous section (Table 4.2, section 4.1).

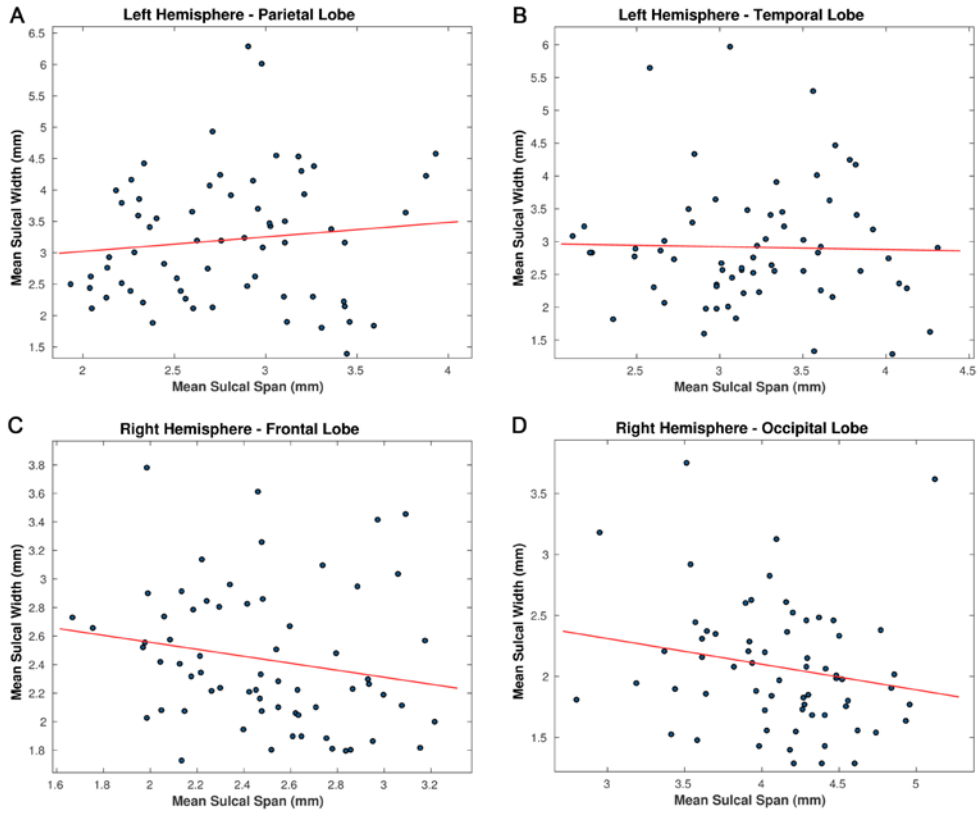

Figure 4.4: *Relationship of sulcal width values computed for both methods SleSA-SW (y axis) and OBM-SS (x axis). The regression line is displayed in* ***red****.*

	Correlation		Regression	
BRAIN LOBES	**r**	**p-value**	**Slope**	**Intercept**
Frontal Left	-0.076	0.544	-0.087	2.882
Frontal Right	-0.189	0.131	-0.245	3.046
Parietal Left	0.113	0.366	0.231	2.558
Parietal Right	0.091	0.470	0.184	2.491
Temporal Left	-0.024	0.845	-0.043	3.051
Temporal Right	-0.155	0.215	-0.249	3.255
Occipital Left	-0.035	0.780	-0.041	2.358
Occipital Right	-0.192	0.123	-0.210	2.941

Table 4.6: *OBM-SS vs. SleSA-SW correlation and regression results for brain lobes.*

Although correlation coefficients are higher than those obtained from OBM-FO vs SleSA-SW correlation analysis, sulcal width and sulcal span values show no significant correlation for any brain lobe. Stronger correlations occur between these two

methods, since their methodology is similar in terms of projecting normal vectors to the sulcal basin's wall to compute the sulcal width.

Secondly, correlation and regression studies are performed for brain sulci. Correlation and regression analyses are performed comparing SleSA sulcal width and OBM fold opening (see Figure 4.5).

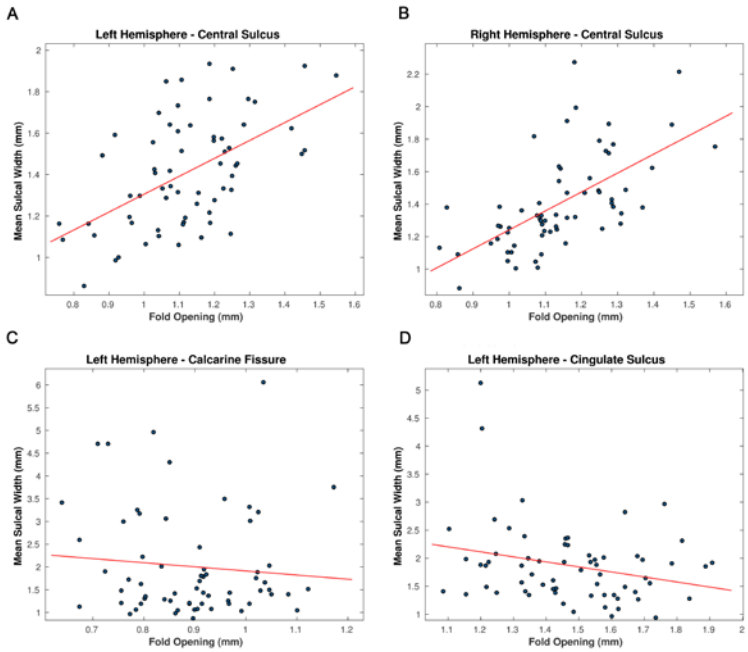

Figure 4.5: *Relationship of sulcal width values computed for both methods SleSA-SW (y axis) and OBM-FO (x axis) for brain sulci. The regression line is displayed in* ***red****.*

	Correlation		Regression	
BRAIN SULCI	**r**	**p-value**	**Slope**	**Intercept**
Central Left	0.539	3.478e-05	0.864	0.441
Central Right	0.616	4.556e-07	1.167	0.073
Cingulate Left	-0.257	0.038	-0.897	3.190
Cingulate Right	-0.157	0.210	-0.587	2.725
Parieto-Occipital Left	-0.098	0.433	-0.025	2.504
Parieto-Occipital Right	-0.077	0.538	-1.008	3.985
Calcarine Left	-0.093	0.457	-0.903	2.816
Calcarine Right	-0.081	0.518	-0.579	2.497
Sup.Temporal Left	-0.042	0.739	-0.385	2.133
Sup.Temporal Right	0.166	0.184	1.270	0.503

Table 4.7: *OBM-FO vs. SleSA-SW correlation and regression results for individual sulci..*

The results obtained show no (linear) correlation between OBM-FO and SleSA. The central sulcus presents an exception. It shows a stronger correlation (0.539 for the left hemisphere and 0.616 for the right hemisphere) and steeper slopes for the regression line that best approximates all data points in linear fashion. The well-defined topology of this sulcus facilitates and guarantees the quality of its basin identification and skeleton extraction as well as its robustness within different subjects, which is the main reason for the aforementioned finding. In fact, fold opening estimations are within a similar range of values as sulcal widths: as seen in Figure 4.5A and Figure 4.5B, sulcal widths go up to 2 mm (if outliers are not taken into account) while fold opening values go up to 1.6mm. For the other sulci the results are different due to the fact that sulcal widths values are higher than fold opening values (see Figure 4.5D). This is because sulcal widths calculation takes into account cases in which one sulcal wall is higher than the opposite sulcal wall, which increases the value of the width, since nodes are further away (larger width magnitude) than the node of the opposite gyral bank they have in their normal direction.

Again, as observed in the t-test analysis (Table 4.3), OBM-FO and SleSA-SW methods are more similar when sulci are compared than when lobes are compared: inter-subject variability is higher in sulci than in lobes.

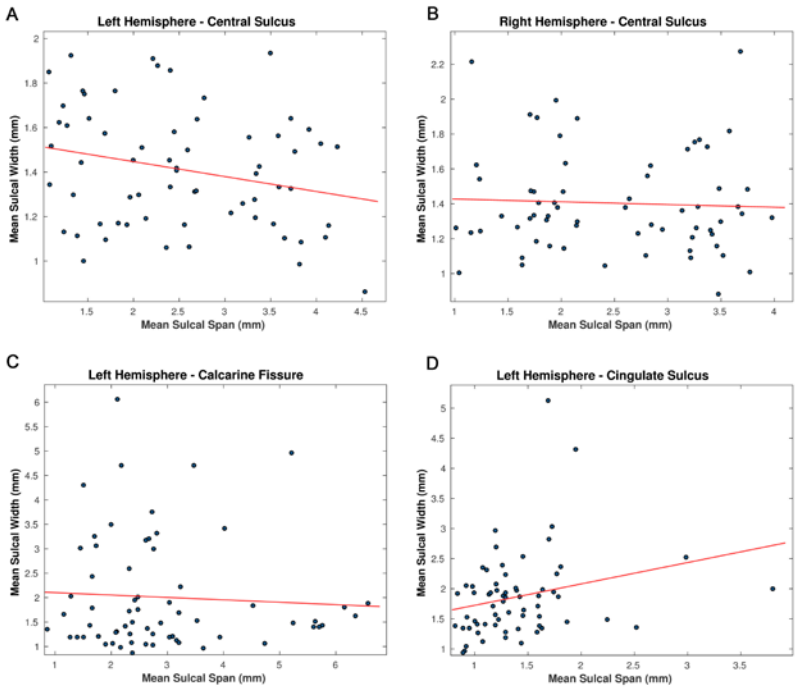

Figure 4.6: *Relationship of sulcal width values computed for both methods SleSA-SW (y axis) and OBM-SS (x axis) for brain sulci. The regression line is displayed in* ***red****.*

	Correlation		Regression	
BRAIN SULCI	**r**	**p-value**	**Slope**	**Intercept**
Central Left	-0.248	0.045	-0.067	1.580
Central Right	-0.046	0.712	-0.015	1.442
Cingulate Left	0.251	0.042	0.355	1.368
Cingulate Right	0.010	0.931	0.024	1.834
Parieto-Occipital Left	0.110	0.380	0.129	2.234
Parieto-Occipital Right	-0.018	0.762	-0.054	3.237
Calcarine Left	-0.060	0.344	-0.049	2.151
Calcarine Right	0.057	0.905	0.043	1.874
Sup.Temporal Left	0.108	0.376	0.055	1.545
Sup.Temporal Right	-0.038	0.402	-0.022	1.802

Table 4.8: *OBM-SS vs. SleSA-SW correlation and regression results for individual sulci.*

As in the previous correlation analysis, these results also show greater correlation between OBM-SS and SleSA-SW. However, sulcal widths have smaller values than sulcal spans. This makes sense because to obtain the sulcal span the Euclidean distance between the two points intersecting the cortical surface at normal directions from the medial mesh is calculated. The problem is that the intersection points can lie on the gray matter mesh of an adjacent sulcal basin, since only measurements from intersections that are further than 4mm from the neighboring sulci are excluded. As a consequence, the resulting Euclidean distance is larger than it should be. This explains why sulcal spans values are larger than sulcal widths.

Given that *r* values are close to zero, there is no correlation between sulcal span and sulcal with in sulci.

4.3. Computation time comparison

Computation time is also important consideration. The methodology should not only be precise and reliable, but it should also minimize its computational time. The average computation time for each subject and each method is presented on this table (Table 4.9).

	OBM-FO	OBM-SS	SleSA-SW
Sulcal Width Computation	0.06 min/subject	7 min/subject	8 min/subject

Table 4.9: *Computation times for the three different algorithms.*

The required time to run the algorithm is similar to that of OBM-SS, which also relies on the use of normal projections to the cortical wall to calculate the width. Extra value is added to our method because it requires less time than OBM-SS (8 minutes/subjects instead of 7 min/subject), although it provides vertexwise sulcal width information.

4.4. Final discussion about the validation

No final conclusions can be extracted from the validation results presented since there is no gold standard to which our methodology can be compared. All previous results were calculated based on the mean sulcal width for the entire sulcus although our proposed method computes the sulcal width of each node of the cortical surface.

Chapter 5: Conclusions and Future Work

5.1. Conclusions

The most important conclusion of this work answers the main objective stated in Chapter 1.3: a methodology that allows for computing a vertexwise sulcal width map over the human cortical surface using magnetic resonance images has been developed. Therefore, it is concluded that:

- Each sulcal basin was divided into different regions according to its anatomical topology using previously extracted sulcal lines and gyral crowns.
- Sulcal depth maps were obtained for each sulcal region.
- Vertex-wise sulcal width maps were computed
- The developed methodology was compared with previous methods

5.2. Limitations

The methodology presented in this work has certain limitations. Some of them need to be considered for future work as addressed in Chapter 5.3. The main limitations in this Project are the following:

- The algorithm has not been tested on images acquired with different scan protocols. The performance of the algorithm strongly depends on the quality of the original image from which the cortical surface is generated. Sulcal lines extraction depends on sulcal parcellation, which is calculated from surface curvature values. This curvature map varies according to the extracted surface.
- The methodology has only been evaluated on healthy patients.
- There is no possible validation since there are no other methods that estimate sulcal width for each point on the cortical surface.

5.3. Future work

A few ideas are presented to solve some of the limitations presented above, as well as ideas for further work.

- Verify robustness by computing the algorithm with data from different databases. It should be tested using control images with lower quality. In

addition, it should also be computed using images not only from controls but also from patients with different pathologies.

- Carry out group comparison studies to estimate the value of sulcal width as a biomarker depending on its change among the different pathologies analyzed.

Appendices

Appendix A: Screenshots of the matlab scripts developed to compute pointwise sulcal width maps.

The following images contain screenshots of the developed matlab functions. Only their header sections are displayed.

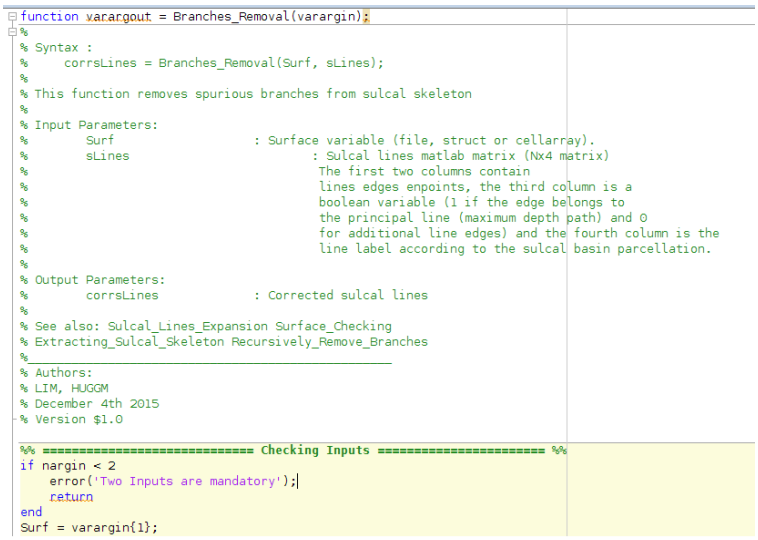

```
function varargout = Branches_Removal(varargin);
%
% Syntax :
%     corrsLines = Branches_Removal(Surf, sLines);
%
% This function removes spurious branches from sulcal skeleton
%
% Input Parameters:
%        Surf                  : Surface variable (file, struct or cellarray).
%        sLines                       : Sulcal lines matlab matrix (Nx4 matrix)
%                                       The first two columns contain
%                                       lines edges enpoints, the third column is a
%                                       boolean variable (1 if the edge belongs to
%                                       the principal line (maximum depth path) and 0
%                                       for additional line edges) and the fourth column is the
%                                       line label according to the sulcal basin parcellation.
%
% Output Parameters:
%        corrsLines            : Corrected sulcal lines
%
% See also: Sulcal_Lines_Expansion Surface_Checking
% Extracting_Sulcal_Skeleton Recursively_Remove_Branches
%_____________________________________________
% Authors:
% LIM, HUGGM
% December 4th 2015
% Version $1.0

%% ============================ Checking Inputs ======================== %%
if nargin < 2
    error('Two Inputs are mandatory');
    return
end
Surf = varargin{1};
```

Figure A.1: *Screenshot of the matlab function employed to remove undesired sulcal line branches.*

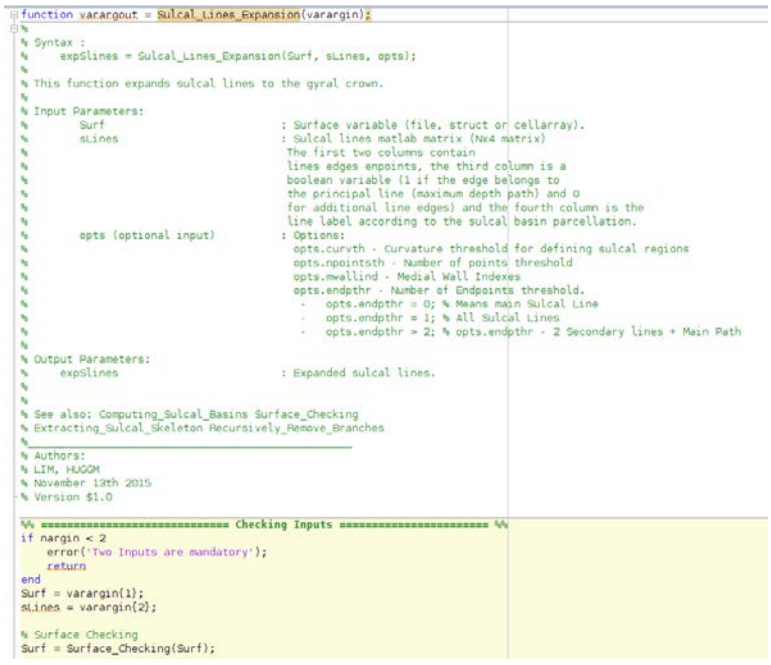

```
function varargout = Sulcal_Lines_Expansion(varargin);
%
% Syntax :
%     expSlines = Sulcal_Lines_Expansion(Surf, sLines, opts);
%
% This function expands sulcal lines to the gyral crown.
%
% Input Parameters:
%        Surf                          : Surface variable (file, struct or cellarray).
%        sLines                        : Sulcal lines matlab matrix (Nx4 matrix)
%                                        The first two columns contain
%                                        lines edges enpoints, the third column is a
%                                        boolean variable (1 if the edge belongs to
%                                        the principal line (maximum depth path) and 0
%                                        for additional line edges) and the fourth column is the
%                                        line label according to the sulcal basin parcellation.
%        opts (optional input)         : Options:
%                                         opts.curvth - Curvature threshold for defining sulcal regions
%                                         opts.npointsth - Number of points threshold
%                                         opts.mwallind - Medial Wall Indexes
%                                         opts.endpthr - Number of Endpoints threshold.
%                                          -   opts.endpthr = 0; % Means main Sulcal Line
%                                          -   opts.endpthr = 1; % All Sulcal Lines
%                                          -   opts.endpthr > 2; % opts.endpthr - 2 Secondary lines + Main Path
%
% Output Parameters:
%     expSlines                       : Expanded sulcal lines.
%
%
% See also: Computing_Sulcal_Basins Surface_Checking
% Extracting_Sulcal_Skeleton Recursively_Remove_Branches
%_____________________________________________
% Authors:
% LIM, HUGGM
% November 13th 2015
% Version $1.0

%% ============================ Checking Inputs ======================== %%
if nargin < 2
    error('Two Inputs are mandatory');
    return
end
Surf = varargin{1};
sLines = varargin{2};

% Surface Checking
Surf = Surface_Checking(Surf);
```

Figure A.2: *Screenshot of the matlab function employed to expand the sulcal line.*

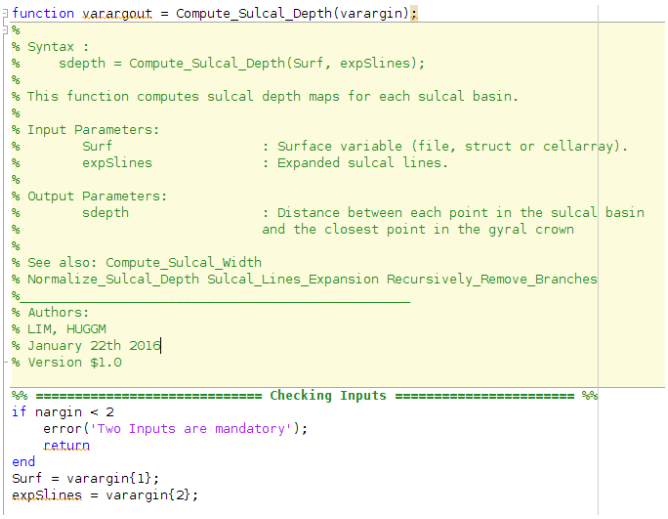

```
function varargout = Compute_Sulcal_Depth(varargin);
%
% Syntax :
%     sdepth = Compute_Sulcal_Depth(Surf, expSlines);
%
% This function computes sulcal depth maps for each sulcal basin.
%
% Input Parameters:
%        Surf                   : Surface variable (file, struct or cellarray).
%        expSlines              : Expanded sulcal lines.
%
% Output Parameters:
%        sdepth                 : Distance between each point in the sulcal basin
%                                 and the closest point in the gyral crown
%
% See also: Compute_Sulcal_Width
% Normalize_Sulcal_Depth Sulcal_Lines_Expansion Recursively_Remove_Branches
%_____________________________________________
% Authors:
% LIM, HUGGM
% January 22th 2016
% Version $1.0

%% ============================ Checking Inputs ======================== %%
if nargin < 2
    error('Two Inputs are mandatory');
    return
end
Surf = varargin{1};
expSlines = varargin{2};
```

Figure A.3: *Screenshot of the matlab function employed to compute sulcal depth maps for individual sulcus.*

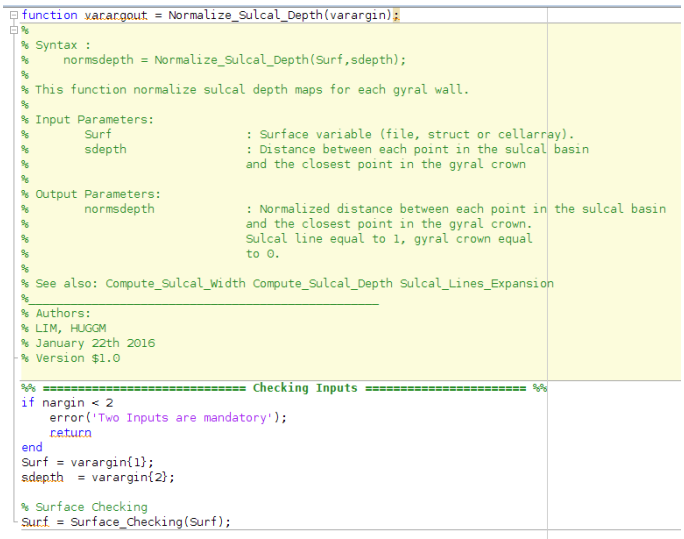

```
function varargout = Normalize_Sulcal_Depth(varargin);
%
% Syntax :
%     normsdepth = Normalize_Sulcal_Depth(Surf,sdepth);
%
% This function normalize sulcal depth maps for each gyral wall.
%
% Input Parameters:
%        Surf                   : Surface variable (file, struct or cellarray).
%        sdepth                 : Distance between each point in the sulcal basin
%                                 and the closest point in the gyral crown
%
% Output Parameters:
%        normsdepth             : Normalized distance between each point in the sulcal basin
%                                 and the closest point in the gyral crown.
%                                 Sulcal line equal to 1, gyral crown equal
%                                 to 0.
%
% See also: Compute_Sulcal_Width Compute_Sulcal_Depth Sulcal_Lines_Expansion
%_____________________________________________
% Authors:
% LIM, HUGGM
% January 22th 2016
% Version $1.0

%% ============================ Checking Inputs ======================== %%
if nargin < 2
    error('Two Inputs are mandatory');
    return
end
Surf = varargin{1};
sdepth  = varargin{2};

% Surface Checking
Surf = Surface_Checking(Surf);
```

Figure A.4: *Screenshot of the matlab function employed to normalize sulcal depth values. Gyral crown points will have a depth value equal to 0 and sulcal line points depth is fixed to 1.*

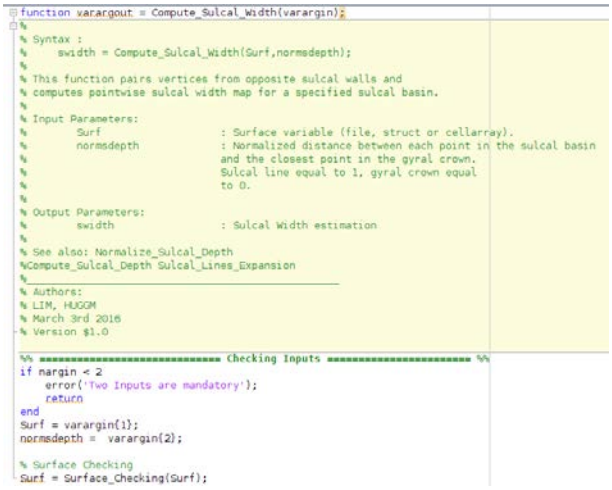

```
function varargout = Compute_Sulcal_Width(varargin);
%
% Syntax :
%     swidth = Compute_Sulcal_Width(Surf,normsdepth);
%
% This function pairs vertices from opposite sulcal walls and
% computes pointwise sulcal width map for a specified sulcal basin.
%
% Input Parameters:
%        Surf                   : Surface variable (file, struct or cellarray).
%        normsdepth             : Normalized distance between each point in the sulcal basin
%                                 and the closest point in the gyral crown.
%                                 Sulcal line equal to 1, gyral crown equal
%                                 to 0.
%
% Output Parameters:
%        swidth                 : Sulcal Width estimation
%
% See also: Normalize_Sulcal_Depth
%Compute_Sulcal_Depth Sulcal_Lines_Expansion
%_____________________________________________
% Authors:
% LIM, HUGGM
% March 3rd 2016
% Version $1.0

%% ============================ Checking Inputs ======================== %%
if nargin < 2
    error('Two Inputs are mandatory');
    return
end
Surf = varargin{1};
normsdepth =  varargin{2};

% Surface Checking
Surf = Surface_Checking(Surf);
```

Figure A.5: *Screenshot of the matlab function employed to compute sulcal width maps.*

Appendix B: Sulci labeling

Labelled regions have a direct application in characterizing the morphometry of the brain. The human barin cortex presents high variability, which difficults its labeling. In 2012, (Klein & Tourville, 2012) develop a surface-based cortical labeling protocol.

The first step in this protocol generates cortical surfaces from previously segmented T1-weighted MRI images using FreeSurfer. FreeSurfer also labels the generated cortical surface using its own cortical parcellations atlas. Labels are then assigned to every point on the cortical surface according to the local surface curvature and convexity and prior analysis of neighboring nodes labels. Sulcal regions are then created from the boundaries between these labeled regions.

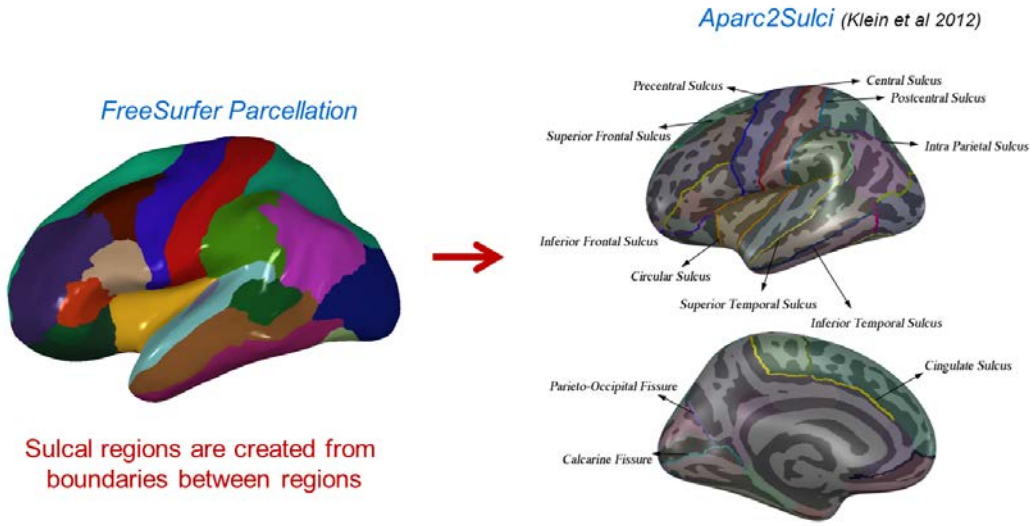

Figure B.1: *Sulci labeling protocol based on FreeSurfer cortical parcellation.*

Related references

Ackerman, S. (1992). *Discovering the Brain*. *Sciences-New York*.

Ashburner, J., & Friston, K. J. (2005). Unified segmentation. *NeuroImage*, *26*(3), 839–851.

Bastos-Leite, A. J., van Waesberghe, J. H., Oen, A. L., van der Flier, W. M., Scheltens, P., & Barkhof, F. (2006). Hippocampal sulcus width and cavities: comparison between patients with Alzheimer disease and nondemented elderly subjects. *AJNR Am J Neuroradiol*, *27*(10), 2141–2145.

Coyle, T. R., Kochunov, P., Patel, R. D., Nery, F. G., Lancaster, J. L., Mangin, J. F., … Soares, J. C. (2006). Cortical sulci and bipolar disorder. *Neuroreport*, *17*(16), 1739–1742.

Dijkstra, E. W. (1959). A note on two problems in connexion with graphs. *Numerische Mathematik*, *1*(1), 269–271.

Fischl, B., Salat, D. H., Busa, E., Albert, M., Dieterich, M., Haselgrove, C., … Dale, A. M. (2002). Whole Brain Segmentation: Neurotechnique Automated Labeling of NeuroanatomicalStructures in the Human Brain. *Neuron*, *33*(3), 341–355.

Fischl, B., Sereno, M. I., & Dale, A. M. (1999). Cortical surface-based analysis. II: Inflation, flattening, and a surface-based coordinate system. *Neuroimage*, *9*(2), 195–207.

Fix, J. D. (1995). *Neuroanatomy*. *Board review series* (2nd ed.). Baltimore: Williams & Wilkins.

Greve, D. N. (2011). An absolute beginner's guide to surface-and voxel-based morphometric analysis. In *Proc Intl Soc Mag Reson Med* (Vol. 19).

Herrmann, N., Harimoto, T., Balshaw, R., & Lanctot, K. L. (2015). Risk Factors for Progression of Alzheimer Disease in a Canadian Population: The Canadian Outcomes Study in Dementia (COSID). *Can J Psychiatry*, *60*(4), 189–199.

Hurd, M. D., Martorell, P., & Langa, K. M. (2013). Monetary costs of dementia in the United States. *N Engl J Med*, *369*(5), 489–490.

Johnson, I. P. (2015). Age-related neurodegenerative disease research needs aging models. *Front Aging Neurosci*, *7*, 168.

Jouvent, E., Mangin, J. F., Duchesnay, E., Porcher, R., During, M., Mewald, Y., … Chabriat, H. (2012). Longitudinal changes of cortical morphology in CADASIL. *Neurobiol Aging*, *33*(5), 1002.e29–36.

Klein, A., & Tourville, J. (2012). 101 Labeled Brain Images and a Consistent Human Cortical Labeling Protocol. *Frontiers in Neuroscience*, *6*(DEC), 1–12.

Kochunov, P., Rogers, W., Mangin, J.-F., & Lancaster, J. (2012, January). A Library of Cortical Morphology Analysis Tools to Study Development, Aging and Genetics of Cerebral Cortex. *Neuroinformatics*.

Koutsouleris, N., Gaser, C., Patschurek-Kliche, K., Scheuerecker, J., Bottlender, R., Decker, P., … Meisenzahl, E. M. (2012). Multivariate patterns of brain-cognition associations relating to vulnerability and clinical outcome in the at-risk mental states for psychosis. *Human Brain Mapping*, *33*(9), 2104–2124.

Le Troter, A., Auzias, G., & Coulon, O. (2012). Automatic sulcal line extraction on cortical surfaces using geodesic path density maps. *NeuroImage*, *61*(4), 941–949.

Li, G., Guo, L., Nie, J., & Liu, T. (2010). An automated pipeline for cortical sulcal fundi extraction. *Medical Image Analysis*, *14*(3), 343–359.

Liang, Z. P., Lauterbur, P. C., in Medicine, I. E., & Society, B. (2000). *Principles of Magnetic Resonance Imaging: A Signal Processing Perspective*. SPIE Optical Engineering Press.

Liu, T., Wen, W., Zhu, W., Kochan, N. A., Trollor, J. N., Reppermund, S., … Sachdev, P. S. (2011). The relationship between cortical sulcal variability and cognitive performance in the elderly. *NeuroImage*, *56*(3), 865–873.

Mangin, J., Frouin, V., Régis, J., & Bloch, I. (1996). Towards better management of cortical anatomy in multi-modal multi-individual brain studies. *Physica Medica*, *12*(January), 103–107.

Mangin, J.-F., Jouvent, E., & Cachia, A. (2010). In-vivo measurement of cortical morphology: means and meanings. *Current Opinion in Neurology*, *23*(4), 359–367.

Martola, J., Stawiarz, L., Fredrikson, S., Hillert, J., Bergström, J., Flodmark, O., … Kristoffersen Wiberg, M. (2008). Rate of Ventricular Enlargement in Multiple Sclerosis: A Nine-Year Magnetic Resonance Imaging Follow-up Study. *Acta Radiologica*, *49*(5), 570–579.

Morris, S., Patel, N., Baio, G., Kelly, L., Lewis-Holmes, E., Omar, R. Z., … Livingston, G. (2015). Monetary costs of agitation in older adults with Alzheimer's disease in the UK: prospective cohort study. *BMJ Open*, *5*(3), e007382.

Nam, K. W., Castellanos, N., Simmons, A., Froudist-Walsh, S., Allin, M. P., Walshe, M., … Nosarti, C. (2015). Alterations in cortical thickness development in preterm-born individuals: Implications for high-order cognitive functions. *NeuroImage*, *115*, 64–75.

Pirttilä, T., Järvenpää, R., Dastidarm, P., & Frey, H. (1993). Brain Atrophy in Neurodegenerative Diseases. *Acta Radiologica*, *34*(3), 296–302.

Schaer, M., Cuadra, M. B., Schmansky, N., Fischl, B., Thiran, J.-P., & Eliez, S. (2012). How to Measure Cortical Folding from MR Images: a Step-by-Step Tutorial to Compute Local Gyrification Index. *Journal of Visualized Experiments : JoVE*.

Shattuck, D. W., Joshi, A. A., Pantazis, D., Kan, E., Dutton, R. A., Sowell, E. R., … Leahy, R. M. (2009, April). Semi-automated method for delineation of landmarks on models of the cerebral cortex. *Journal of Neuroscience Methods*.

Strimbu, K., & Tavel, J. A. (2010, November). What are Biomarkers? *Current Opinion in HIV and AIDS*.

Suetens, P. (2009). *Fundamentals of Medical Imaging*. Cambridge University Press.

Van Essen, D. C., Ugurbil, K., Auerbach, E., Barch, D., Behrens, T. E. J., Bucholz, R., … Yacoub, E. (2012, October). The Human Connectome Project: A data acquisition perspective. *NeuroImage*.

Van Soelen, I. L. C., Brouwer, R. M., Van Baal, G. C. M., Schnack, H. G., Peper, J. S., Collins, D. L., … Hulshoff Pol, H. E. (2012). Genetic influences on thinning of the cerebral cortex during development. *NeuroImage*, *59*(4), 3871–3880.